Anatomy and dynamics of a mixed contourite sand sheet, Ryukyu Island Arc, northwestern Pacific Ocean

Naohisa Nishida[1, 2]*, Takuya Itaki[2], Atsuko Amano[2], Hajime Katayama[2], Taichi Sato[2], Dorrik Stow[3], Uisdean Nicholson[3]

[1]Department of Environmental Sciences, Tokyo Gakugei University, Koganei, Tokyo 184-8501, Japan

[2]Geological Survey of Japan, AIST, Tsukuba, Ibaraki 305-8567, Japan

[3] Institute of GeoEnergy Engineering, School of Energy, Geoscience, Infrastructure and Society (EGIS), Heriot-Watt University, Edinburgh, EH7 4JA, UK

*Corresponding author: nishidan@u-gakugei.ac.jp

ABSTRACT

Contourites are well-known from many continental margins under the influence of bottom currents but have been little reported from the Pacific Ocean. This paper documents a new area of contourite-controlled sedimentation in the NW Pacific Ocean, which we call the *Ryukyu Sand Sheet*. This contourite sand sheet has an area of around 35,000 km^2 and extends from the narrow island shelves to over 1500 m water depth. It comprises mainly moderate to well-sorted fine-grained sands, with current ripples and giant sediment waves and is also associated with small drifts. It is formed under the influence of three principal current systems – the Kuroshio Current, the Kuroshio Countercurrent and the Ryukyu Current. The interaction of these currents with each other and with a complex seafloor topography, spawns a series of meso-scale gyres, eddies and vortices that shape the seafloor and lead to deposition of an extensive sandy substrate, locally with gravels and exposed seafloor. Strong surface currents, as well as deep-water thermohaline circulation, both influence the depositional and erosional processes of deep-sea sediments. The role of the modern Kuroshio Current in this context supports earlier work that proposed an ancestral Kuroshio Current for the deposition of Miocene contourites onshore Japan. Sediment supply to the Ryukyu Sand Sheet is by a mixed process of seafloor polishing and sand spillover that involves combined oceanographic and gravitational processes.

Keywords

Kuroshio Current; Ryukyu sand sheet; Okinawa Trough; sandy contourite; sediment waves

1. Introduction

Contourites, deposited under the influence of bottom currents, are a major feature of deep-sea sedimentary environments (Stow and Faugères 1993; Stow et al., 2002a, b; Rebesco and Camerlenghi, 2008; Rebesco et al., 2014). They typically occur in continental slope and abyssal plain settings (Hernandez-Molina et al., 2008a, b), commonly associated with sediment gravity-flow deposits (e.g., turbidites and debrites), hemipelagites and pelagites in mixed depositional systems (Stow and Faugères, 1998; Mulder et al., 2008; Rebesco et al., 2014; Brackenridge et al., 2020). They also occur in more shallow water settings on the outer shelf and upper slope, although this context is less well known (Armishaw et al., 1998; Viana et al., 1998; Verdicchio and Trincardi, 2008).

Studies in the last two decades have greatly advanced our understanding of contourites, including their facies characteristics, the depositional and erosional processes beneath bottom currents, and the principal controls that affect their nature and occurrence (climate, sea level, sediment supply and tectonics) (Stow et al., 2002b; 2018; Rebesco and Camerlenghi, 2008; Hernández-Molina et al., 2014, 2016; Rebesco et al., 2014; Lasabuda et al., 2018; Smillie et al., 2018; Stow and Smillie, 2020). The economic, paleoceanographic and hazard significance of contourites is equally well recognised (Viana and Rebesco, 2007; Knutz, 2008; Laberg and Camerlenghi, 2008; Brackenridge et al., 2020).

Recent studies have also shown that strong surface currents, and in particular the presence of high-velocity meso-scale eddies can impact the seabed at depths of hundreds of metres to several kilometres (Gardner et al., 2017; Nicholson and Stow, 2019; Nicholson et al., 2020; Davies et al., 2021). In such settings, eddies can temporally increase water velocities by an order of magnitude (Sheen et al., 2012; Gardner et al., 2017), resulting in winnowing, erosion and redistribution of sediment. This can result in the formation of extensive sand sheets, such as the Falkland Sand Sheet in the South Atlantic (Nicholson and Stow, 2019) and the Cadiz Sand Sheet in the eastern North Atlantic (Stow et al., 2013a, b).

However, despite these growing number of contourite studies, and despite major wind-blown and thermohaline-driven circulation being well established in the Pacific

(Broecker, 1991; Talley et al., 2011; Talley, 2013), there is a relative paucity of data on Pacific Ocean contourites (Faugères et al., 1993; Rebesco, 2005; Stow and Faugères, 2008; Rebesco et al., 2014; Zhao and Liu, 2017; Brackenridge et al., 2020). Examples include the Samoan Passage, southwest Pacific (Lonsdale, 1981), and Horizon Guyot in the central Pacific (Lonsdale et al., 1972). In the North Pacific, deposits on the continental shelf (14–96 m water depth) and slope (340–800 m water depth) around Miyakojima Island, southern Japan (Tsuji, 1993), have been regarded as tide-influenced contourites (Viana et al., 1998; Rebesco et al., 2014). A field of sand dunes, waves and ribbons has formed under the influence of the Kuroshio Current as it sweeps across the Izu Ridge (200–400 m water depth) (Kubo et al., 2004). We interpret these as shallow-water contourites. In addition, geophysical studies and numerical modeling have identified a contourite drift in the South China Sea, along the central western Pacific margin (Palamenghi et al., 2015; Chen et al., 2016, 2021).

This paper presents a new interpretation of previously collected sediment samples, geophysical and oceanographic data from an area around the central Ryukyu Islands, southwest Japan, in the northwestern Pacific Ocean, influenced by the Kuroshio and Ryukyu currents. We address three important topics in contourite research: (a) the documentation of a new contourite depositional system in the Pacific Ocean, which we call the *Ryukyu Sand Sheet*; (b) the influence of strong wind-driven currents, thermohaline currents, and high-energy meso-scale gyres, eddies and vortices on sandy contourite deposition; and (c) the interpretation of the sand sheet as the result of mixed contourite, turbidite and shelf spillover processes.

2. Regional setting

2.1. Geological framework

The Ryukyu island arc is situated between forearc (Ryukyu Trench) and back-arc (Okinawa Trough) basins formed by the subduction of the Philippine Sea plate beneath the Eurasia plate. The island chain is divided into northern, central, and southern parts by the Tokara Strait and the Kerama Gap. This study focuses on the central region

around Amami-Oshima, Tokunoshima, and Okinawa islands (Fig. 1A). On the eastern side of the islands, the seafloor slopes steeply, with a local gradient up to 10°, toward the Ryukyu Trench, which reaches a water depth in excess of 5000 m. The slope is dissected by several large submarine canyons, with head regions incising into the upper slope at a water depth of 200–300 m, and by numerous smaller slope channels that initiate on the slope at between 500–800 m. The seafloor on the western side of the islands is characterised by numerous small basins and intervening highs leading down to the Okinawa Trough at a water depth of around 1500 m (Itaki, 2015) (Fig. 1B).

2.2. Oceanographic setting

The *Kuroshio Current*, which is the western boundary current of the North Pacific subtropical gyre, has a current velocity of up to 1–2 m s^{-1} (Taft, 1978) and transports an average volume of 25 Sverdrups (Sv) (Kamidaira et al., 2017). The current flows across the continental slope east of Taiwan, where it causes substantial erosion of the seabed (Das et al., 2021). It enters the Ryukyu region through the channel east of Taiwan, flows along the Okinawa Trough, and exits the region via the Tokara Strait (Fig. 1A). The current meanders significantly, and cyclonic and anticylonic meso-scale (~100 km diameter) eddies are a common feature (Kawabe, 1995; Hsin et al., 2008). Recent evidence shows that the Kuroshio Current, and particular associated eddies, are strengthening in response to warming surface waters and enhanced tropical storm events (Zhang et al., 2020).

The current also interacts with shallow bathymetric features, resulting in the formation of sub-mesoscale vortices, particularly in the lee of islands in the Ryukyu region (Hsu et al., 2017). These Island-Induced Ocean Vortex Trains also affect the seabed hundreds of metres below the ocean surface. Numerical models predict significantly elevated Eddy Kinetic Energy and vorticity around the Ryukyu Islands (Kamidaira et al., 2017) (Fig. 1C, D).

Oceanographic studies have revealed that a countercurrent flows beneath the Kuroshio Current (Lie et al., 1998; Nakamura et al., 2008). This *Kuroshio Countercurrent* is caused by the Neptune effect, an eddy-topography interaction that induces current flow (Holloway, 1992), when the turbulent, unstable Kuroshio Current encounters the

sloping seafloor topography at the northern end of the Okinawa Trough (Nakamura et al., 2008).

To the south-east of the Ryukyu Islands, the *Ryukyu Current* is the dominant current system (Fig. 1A, B). The core of this north-east flowing current is at around 700–1000 m water depth, where average velocities exceed 10 cm s^{-1} (Thoppil et al., 2016; Zhao et al., 2020). This current is also affected by meso-scale eddies, and near-seabed velocities exceeding 80 cm s^{-1} have been measured by Acoustic Doppler Current Profilers to the south-east of Okinawa during the passage of such events (Konda et al., 2005). Elevated velocities associated with the Ryukyu Current are also predicted to occur in the deeper passages separating the Ryukyu Islands (Thoppil et al., 2016) (Fig 1D). In addition to the major currents, strong currents regionally have been also observed. In the Kerama Gap, which is the deepest strait connecting the East China Sea and the Pacific Ocean, strong and steady currents 50 m above the seafloor (at an instrument depth of 1366 m depth) flowing north-northeastward along the 1400 m isobath with a mean speed of about 25.6 cm s^{-1} have been measured by using a CTD, Argo float profile data, and current-meter moorings (Nakamura et al., 2013).

The interaction of the Ryukyu Current and Kuroshio Current (and counter current) in these areas is likely to result in more complex sub-mesoscale vorticity as observed in the south-western islands. The impact of these currents on seafloor sediments has not previously been documented.

3. Materials and methods

Sediment samples and geophysical observation data were collected during cruises GH08, GH09, GH10, GK12, GK14, GH15, and GK15-2 conducted by the Geological Survey of Japan, National Institute of Advanced Industrial Science and Technology during 2008 to 2015. The sediment samples were collected with grab samplers at 642 stations. The samples are mainly sand and mud, as well as gravel.

Compositionally, the sand and mud are characterised by calcareous bioclastics derived from shells, pteropods, bryozoans, foraminifers, rhodoliths, and corals, with minor lithogenic and volcanic grains (Itaki, 2015). Chemical composition of the samples

are dominated by CaO (11.01–47.56 wt%) with minor Al_2O_3, K_2O, TiO_2, MgO, Total-Fe_2O_3 Tio2, T-Fe2O3, Sc, V, Co, and Zn (Ohta et al., 2013, 2016), which is consistent with the grain composition.

At each station, seafloor photographs were taken with deep-sea cameras (model 371, Benthos Inc., USA, and a RICOH GR-based system, Ocean Engineering Research, Inc., Japan) attached to the grab sampler. Subsamples were obtained from the sediment samples by using a plastic case (6 cm × 5 cm × 30 cm) (named sub-core) on the ship. The seafloor photographs were examined for ripple morphology and indications of current direction. The current flow direction was inferred from the orientation of the ripple crest and grain size asymmetry with respect to the crest by referring to a compass attached to the grab sampler. If no grain size asymmetry was recognised, only the sense of the current flow was determined. The wavelength of the ripples in the center of each photograph was estimated by comparison with the compass (length, 40 cm).

Detailed seafloor bathymetry was conducted with a multi-beam echo sounding system (EM122, Kongsberg Maritime AS, Kongsberg, Norway, freq. of 12 kHz). The sound velocity correction used real-time data from the surface water velocity meter and the sound velocity profiles collected by conductivity, temperature, and depth (CTD), expendable CTD (XCTD), and expendable bathythermograph (XBT) observations in the study area. Anomalous depth variations mainly from the outer edges of the multi-beam swaths were removed by using HIPS and SIPS software (CARIS, Ltd., Fredericton, Canada). The resultant maps use scientific color scales (Crameri, 2018). Sub-bottom profiler (SBP) data were acquired by using the ATLAS ParaSound P70 echosounder. The SBP system adopts a parametric effect. The primary high frequency and the secondary low frequency were 20 kHz and 4 kHz, respectively. Pulse length was 0.5 msec, and beam width was 4×4.5 degree. Ship speed was about 9 knots for the SBP survey. Bandpass filtering and gain control were applied to obtained profiles using ATLAS PARASTORE.

In addition, bedform formation was observed in seafloor videos shot by a remotely operated vehicle (ROV) (TRITON XLR05, PERRY), and the current velocity of the bottom water, measured previously with an Acoustic Doppler Current Profiler (Nagao et al., 2011), was taken into consideration.

196 Radiocarbon ages were determined from foraminifera in surface sediments (depth:
197 0–2 cm) from sites 221 (water depth of 397 m) and 242 (water depth of 839 m) by
198 Beta Analytic Inc. (Miami, FL, USA). All ages are reported as conventional ^{14}C ages (kyr
199 BP).

200

201 # 4. Results

202

203 ## *4.1. Seafloor morphology*

204

205 The central region of the Ryukyu Island Arc presents a very varied topography,
206 rising from volcanic islands up to 500 m above sea level to basins and troughs at over
207 2000 m below sea level (Fig. 2). Slope gradients range from gentle to flat on the floors
208 of basins or the crests of highs, becoming very steep around the island flanks, as much
209 as 8–10° and even exceeding 30° locally. Multibeam mapping of over of data covering
210 area of over 16,000 km^2 together with high-resolution sub-bottom profiling reveal an
211 equally varied seafloor morphology. The principal features (Figs. 3–7) include:

212 (a) Slope channels – relatively straight, short (5–15 km), and closely-spaced on
213 steeper island flanks.
214 (b) Eroded and abraded surfaces – covering extensive areas of seafloor, with
215 highly-reflective substrate, local reflector truncation, broad scoured lows.
216 (c) Moats and alongslope channels – patch drifts have scoured moats; alongslope-
217 oriented channel segments.
218 (d) Plastered drift and terrace – a large convex-up depositional feature on the
219 slope of the submerged bank (~500 m to > 650 m water depth) northwest of
220 Amami-Oshima Island. This feature actually consists of two separate convex-up
221 bodies separated by a notch and terrace at around 600 m, flanked by a moat on
222 its upslope side.
223 (e) Sheeted basin fill – flat seabed and parallel sub-bottom reflectors on the floor
224 of basinal areas.

225

4.2. Bedforms

There are two main types of bedforms observed in the study area: giant sediment waves, seen with multibeam echosounder and sub-bottom profiling, and current ripples, seen with seafloor photography.

4.2.1. Giant sediment waves

Giant sediment waves are apparent in several areas (Fig. 4). These bedforms are characteristically up to 10 m in amplitude (height), 100–400 m in wavelength (from crest to crest) and are up to 5 km in length along the crest of the bedforms. One large field of waves, to the west of Tokunoshima Island, have a crestal orientation perpendicular or highly oblique (up to 60°) to a south-east dipping slope, at water depths of 750–900 m (Fig. 5). This slope is part of a bathymetric high that is separated from Amami-Oshima Island by a deep trough, where water depth exceeds 1 km. Another field of sediment waves, also with crests oriented perpendicular to the slope, is situated at a similar water depth along a north-west facing slope to the north of Amami-Oshima Island. Slope-parallel bedforms are also evident in this area, mainly in association with slope channels and canyon systems.

Another field of sediment waves is formed to the east of Tokunoshima Island, at water depths of 650–750 m (Fig. 6). These have similar dimensions to those described above, but are oriented parallel to the slope. Several downslope channel segments also contain sediment wave trains, with much shorter crestal extension (< 1 km) across channels, but otherwise with similar amplitude and wavelengths at the lower end of the 100–400 m range. In addition, more complicatedly, sediment waves with crests oriented both perpendicular and parallel to the slope are presented in the west of Amami-Oshima Island at water depths of 700–900 m (Fig. 7).

4.2.2. Current ripples

Ripples were observed over the sandy substrate at 102 stations in water depths ranging from 34 to 1839 m (Fig. 2, Table 1). In plan view, the ripple morphology is commonly straight or sinuous (Fig. 8). These give an indication of current sense, but not direction. Some linguoid ripples are also evident at several stations, and these

more clearly indicate current direction. Mean ripple wavelength is 12.5 cm (*n* = 66 stations), with a range from 7.0–24.1 cm (Table 1). The current direction and ripple sense are highly variable across the region, including downslope, upslope and alongslope (Fig. 2). Some areas show a distinctly alongslope orientation (e.g. east of Amami-Oshima Island), others have an across-slope (either up or downslope) orientation.

4.2.3. Sediment facies and distribution

Three sediment facies are identified – mud, sand and gravel – as well as areas of exposed bedrock at the seafloor. These were documented in preliminary research reports of the Geological Survey of Japan by Itaki et al. (2010, 2011), Amano et al. (2013, 2015), Itaki (2015, 2018), and Nishida et al. (2016). Sand is the dominant facies (Figs. 2 and 9), mostly fine to medium-grained, but the grain size ranges from very fine to coarse sand depending mainly on water depth. The fine and very fine sands are mainly moderately well to well sorted, whereas the medium and coarse sands are moderate to poorly sorted. Distinctive structures are usually not apparent in sub-cores, but parallel and cross-lamination are visible on soft-X radiographs (Fig. 9), with bioturbation evident in many cases. In some sub-cores, both upward fining and upward coarsening is observed, including bi-gradational beds and alternating layers of fine and medium sand (bed thickness 1.0–1.5 cm). There is likely a positive correlation between median grain size and ripple wavelength (Fig. 10).

By comparison, the mud facies show some bioturbation and an absence of primary sedimentary structures. They are mainly clayey silts and silty clays, with very poor sorting. The gravels are poorly recovered and/or disturbed during the coring process.

In the SBP profiles, four types of reflective patterns are recognised (Fig. 3). Type A is characterised by a single, smooth reflection at the seabed. Type B is characterised by single, rough seabed reflection. Type C is characterised by multiple, stratified reflections with discontinuous internal structures. Type D is characterised by multiple, stratified reflections and continuous internal structures, with greater penetration depth than Type C. These facies types are related to surface sediment type and seafloor morphologies. Comparing with Fig. 2, Type A is corresponds to sand deposited on relatively steep slopes. Type B corresponds to coarse-grained sand, gravelly sand

and exposed basement rocks on the shelf, slope and shallow banks. Type C corresponds to sand on slope settings, including the upper portion of a plastered drift where sediment waves are present (Fig. 5). Type D corresponds to silty sand, silt and mud on the basin or in plastered drifts deposits.

The sediment on the seabed around the Ryukyu Islands is dominated by sand – covering an estimated 70% (about 30,000 km^2) of the mapped area (Fig. 2). Mud covers about 17.5% of the area and gravel/bedrock the remaining 12.5%. The sand and gravel cover the seafloor down to a water depth of 700–1000 m, and locally to 1500 m, whereas the mud is mostly confined to deeper mini-basins and open slopes. The mudline (sand-mud boundary), therefore, is generally around 700–1000 m water depth, and locally deeper. Gravel or bedrock is mostly confined to shallow banks (bathymetric highs) at water depths of less than 500 m. Where gravel deposits or exposed bedrock extend into deeper-water, this is almost exclusively to the north-east of individual islands.

4.2.4. Video coverage

Several videos were taken from a Remotely Operated Vehicle at selected stations. These all show active bottom current flows above the sandy substrate at depths up to 700 m (Animation 1, Supplementary Material), consistent with reported bottom current velocities of up to 100 cm s^{-1} measured by Acoustic Doppler Current Profiler west of Okinawa Island (Nagao et al., 2011).

4.2.5. Radiocarbon ages

A radiocarbon ages obtained from foraminifera-rich sands in site 221 (water depth of 397 m) is 13260 yr BP (error: 50 yr BP; Lab ID: Beta-344159). The age for site 242, characterised by ripples (water depth of 839 m), is 19910 yr BP (error: 80 yr BP; Lab ID: Beta-344160). Note that both dates were obtained from foraminiferal material in the top 2 cm of sediment column – see discussion below.

5. Discussion

5.1. Ryukyu Sand Sheet and global context

We describe here for the first time an extensive area of the seabed around the Ryukyu Islands that is dominated by well-sorted, current rippled sand, and that includes some areas of gravel and exposed bedrock. We call this feature the *Ryukyu Sand Sheet* (Fig. 2). It covers an area (including the gravels) of at least 35,000 km^2, which places it as one of the largest known sand sheets anywhere in the deep ocean, comparable in size with the Falkland Sand Sheet in the SW Atlantic (30,000 km^2, Nicholson and Stow, 2019), and considerably larger than the Cadiz Sand Sheet (Stow et al., 2013a, b; Brackenridge et al., 2018) and the Barra Sand Sheet (Stow et al., 2002c) in the North Atlantic. These three cases are examples of contourite sand sheets, controlled principally by the action of strong bottom currents (Table 2).

There are a number of other examples of contourite sand sheets that have been recorded worldwide, and that show a range of features in terms of size, water depth, sediment character and depositional processes involved. A first review of these was presented by Viana et al (1998), in which they denoted three principle settings for their occurrence: (a) deepwater, base-of-slope and basinal (> 2000 m); (b) mid-depth, slope and slope-terrace (300–2000 m); and (c) outer shelf to upper slope (50–300 m). This last category they referred to as outer shelf/upper slope bottom-current sands or shallow-water bottom-current sands, rather than as contourites *sensu stricto*. However, following current usage we prefer to call these *shallow-water contourites*. These examples, as well as a selection of those published more recently, are summarised in Table 2 (see references therein). In most cases, we have introduced specific names for these sandy contourite systems, as indicated in the table.

These sand-rich contourite sheets are mostly from the Atlantic Ocean and occur at the present-day seafloor (i.e. Holocene), although in some cases initiation of the system extends back to the Neogene and even Oligocene (Table 2). They range in size from around 100 km^2 to an estimated 30,000 km^2 for the Falkland contourite sheet, and from outer shelf depths (60 m) to over 3000 m water depth for the Hatton flank sheet. It is more difficult to assess the sandbody thickness, but it appears that these too show a wide range of values, from around 10 m (e.g. Barra sand sheet) to as much as 800 m of interbedded sandstone and mudstone contourites (Cadiz sand sheet). All are sand-dominated, some including pebbly sands and gravels, and having dominantly

siliciclastic or bioclastic or a mixed composition. Those sand sheets in deepwater or mid-water depths are dominantly molded and deposited by a strong bottom current regime, which may include thermohaline bottom currents, major surface currents, and high benthic energy associated with water mass fronts (Rebesco et al., 2014; Stow and Smillie, 2020). The shallow-water systems are controlled by a more complex mix of processes, including a strong upper slope/outer shelf current, mesoscale eddies, storm- and tide-induced currents, and internal waves – see discussion below (5.2).

The Ryukyu Sand Sheet is one of the most distinctive sand sheets worldwide due to not only the extensive area, but also the complex processes influenced by the Kuroshio Current. Several of the larger-scale seafloor morphological features noted in the study area are compatible with a bottom-current origin. These include erosive and abraded surfaces at the seafloor, some of which are in areas that could not be affected by turbidity currents, alongslope channels and moats, and the patch drift, terrace and moat on the flank of the submerged bank west of Tokunoshima Island. The bedforms across the Ryukyu Sand Sheet, fields of giant sediment waves and current ripples, are also interpreted to be formed by bottom currents.

Wave influence on the ripple formation is considered negligible because the water depth at the stations where ripples were observed was generally more than 100 m (average 512 m at 94 stations), except at seven stations (34–97 m) (Table 1). The relationship between grain size and ripple wavelength is consistent with the expected relationship for current ripples formed by a unidirectional current (Allen, 1982). The current direction and ripple sense are highly variable (Fig. 2, Table 1). Ripples to the east of the islands show a more consistent current direction flowing to the north-east, parallel to the contours. We interpret these to have formed under the Ryukyu Current and the sands to be sandy contourites. This is compatible with the ROV videos, which show ripples actively forming under a bottom current system. However, at other stations, a cross-slope current direction or sense is evident, which is more compatible with downslope movement and/or the effects of internal tides.

The distribution and characteristics of the larger scale bedforms (wavelength 100–400 m) in some areas (e.g. Figs. 5 and 7) also suggest the influence of a relatively stable alongslope current. There are many other examples of bottom-current sediment waves in the literature, as summarised by Wynn and Stow (2002), and more recently

highlighted at the foot of the Malta escarpment by Rebesco et al (2021). Across the northern end of the Izu Ridge off SE Japan, a large swathe of asymmetric bedforms (wavelength 50–500 m) has been linked to passage of the Kuroshio Current affecting the seafloor between 200–400 m water depth (Kubo et al., 2004). This sand body we have called the Kozushima sand sheet, and suggest that the wave forms are closely comparable to parts of the Ryukyu Sand Sheet. However, there are other areas where the sediment waves are indicative of a downslope flow direction, both within channels and on the open slope (e.g. Figs. 6 and 7). It seems clear that the processes responsible for the mobilisation, transport and deposition of sand across the Ryukyu Sand Sheet are complex and include down-slope gravity currents, alongslope bottom currents, as well as the range of processes involved in seafloor polishing and sediment spillover (Viana et al., 1998; Stow and Mayall, 2000). This is discussed further below.

5.2. Mixed Process System

We consider, therefore, that the Ryukyu Sand Sheet has formed as a mixed process system, with distinct and interacting components of alongslope (bottom currents), downslope, seafloor polishing and spillover.

5.2.1. Bottom currents

The Ryukyu Island chain is under the influence of three important current systems – the Kuroshio Current, the Kuroshio Countercurrent and the Ryukyu Current (Lie et al., 1998; Nakamura et al., 2008; Thoppil et al., 2016). All three currents are capable of directly affecting the seafloor and its sediment cover to depths in excess of 1000 m (Taft, 1978). The effects of the Kuroshio Countercurrent are noted at 2200 m depth in the Okinawa Trough (Lie et al., 1998; Nakamura et al., 2008). Equally significant for energy kinetics at the seafloor are the subordinate gyres, meso-scale eddies and sub-mesoscale vortices (Nakamura et al., 2008; Thoppil et al., 2016; Hsu et al., 2017). The estimated maximum current velocity in the subordinate gyres is 10–20 cm s^{-1} at 520 m water depth (Nakamura et al., 2008), and up to 80 cm s^{-1} near the seabed at 700–1000 m depth (Konda et al., 2005). Both the observed ripples and giant sediment waves can be formed under these variable current conditions (Stow et al., 2009).

418 The two radiocarbon ages were taken from material at the sediment surface (0–2
419 cm) and yet showed dates of 13,260 and 19,910 y BP. Both sites have a sandy
420 substrate and show no evidence of clear downslope transport, either from local
421 seafloor morphology or from the sub-core sample. It is therefore likely that these
422 relatively old dates indicate that extensive winnowing and reworking by bottom
423 currents has taken place at these sites, probably associated with erosion and/or non-
424 deposition. Although the sample number of two is very limited, it may further suggest
425 that the Ryukyu Sand Sheet has been formed under the influence of strong bottom
426 currents since around the Last Glacial Maximum to the early Holocene.

427 The dominance of sand facies across the entire region we interpret as the result of
428 elevated energy kinetics under these deep-acting surface and bottom-currents. The
429 interaction of the Kuroshio Current, Kuroshio Countercurrent and incursions of the
430 Ryukyu Current, and with the complex seafloor topography of the Ryukyu Island chain
431 likely leads to the formation of numerous subordinate gyres, eddies and vortices,
432 capable of winnowing and transporting sand. This may also account for the wide
433 distribution of current measurements observed in the region.

434 The large convex-up depositional bodies observed on sub-bottom profiler (Fig. 3)
435 are consistent with the geometry typical of a plastered contourite drift separated by a
436 narrow terrace (Faugères et al., 1999; Faugères and Stow, 2008; Rebesco et al., 2014).
437 Although such drifts are typically mud-dominated, silt or sand layers are relatively
438 common (Hernández-Molina et al., 2008a, b), and some may be plastered sandy drifts
439 (Stow et al., 2002c). The only sample obtained from this dual drift is from near the
440 'notch' and is a fine-medium sand. We interpret this notch as a moat on a terrace
441 between the two plastered drifts, representing the core (highest velocities) of the
442 current. This dual drift feature has enhanced reflectivity below the seabed compared
443 to other areas, which may indicate that it is finer-grained than surrounding sediments.
444 As the Coriolis effect results in sediment being preferentially deposited to the right
445 (relative to the direction of transport) of the current core in the northern hemisphere,
446 we suggest that this drift is primarily formed under the north-east flowing Kuroshio
447 Current, rather than the south-west flowing Kuroshio Countercurrent.

448 The distribution of gravels, or exposed bedrock, on the local bathymetric highs
449 (>500 m) east of the islands suggests that these are actively winnowed by strong,

relatively shallow currents on the northeast side of the islands. This is shallower than the observed depths of the Kuroshio Countercurrent. We suggest that these are winnowed by the meandering main Kuroshio Current, or by meso-scale eddies formed in association with this current. Eddies formed at other large surface currents, such as the Antarctic Circumpolar Current, are capable of causing widespread erosion in relatively deep water (Nicholson and Stow, 2019). Further to the south, offshore Taiwan, widespread erosion is also associated with the Kuroshio Current as it interacts with the Kenting Plateau at intermediate (400–700 m) water depths (Das et al., 2021).

The distribution of gravels in deeper water (>500 m) shows a characteristic pattern, being confined almost entirely to the northeast of individual islands, with mud typically deposited to the north or northwest of the islands. We suggest that this is a result of island-induced ocean vortices forming in the lee of the islands, as observed in the Kuroshio Current to the northwest of Taiwan (Hsu et al., 2017). This suggests that these are also predominantly formed by the northeast flowing Kuroshio surface current rather than the Kuroshio Countercurrent.

5.2.2. Downslope processes

Normal downslope processes are also active in the region, as clearly visible from multibeam mapping, including the presence of canyons and slope channels, and the sheeted fill of mini-basin floors. Turbidity currents and debris flows are therefore responsible for the supply of some of the sediment to deeper water. Turbidites, and potentially also Mass Transport Deposits (MTDs) will occur interbedded with contourite sand sheet and mud-rich drifts. In other cases, individual turbidites are most likely wholly reworked by bottom currents. The characteristic sediment waves field in the west of Amami-Oshima Islands (Fig. 7) is interpreted to result from the interaction of bottom currents and downslope processes.

5.2.3. Seafloor polishing and spillover

The Ryukyu Sand Sheet represents the drape of relatively coarse-grained sediment across the shelf, outer shelf and slope, in some places to a depth of at least 1500 m. We infer that the supply of sandy sediment across shelf and into deeper water is by a mixed process of seafloor polishing and sand spillover (Viana et al., 1998; Armishaw et

al., 2000; Stow and Mayall, 2000). The admixture of bioclastic and lithic (volcaniclastic) sands in shallow water surrounding the islands is cleaned, winnowed and sorted by the combined action of wave and tidal processes, shelf currents and eddies (i.e. seafloor polishing). The strong action of the Kuroshio Current is noted on the continental shelf sands beneath its main pathway and branches (Ikehara and Kinoshita, 1994; Kubo et al., 2004; Nishida and Ikehara, 2013; Nishida et al., 2020). These sands are then transported across shelf and downslope by a combination of internal tides and waves, meso-scale current gyres, eddies and vortices, sediment re-suspension, downslope creep and unconfined turbidity currents (i.e. spillover processes).

These spillover processes have been demonstrated for other bottom-current controlled sands systems (Table 2), including the Campos Basin slope in the SW Atlantic (Viana et al., 1998, 2002), and the Hebridean slope (Armishaw et al., 2000; Stow et al., 2002c). Preu et al. (2011) have demonstrated the process in action off the Mozambique outer shelf to slope, by re-processing multibeam echosounder and ACDP data for imaging the water column. Whereas the sand-mud transition (the mudline) typically occurs close to the shelf-slope boundary on many continental margins, the extension of the mudline further downslope, as shown here for the Ryukyu Sand Sheet, is the result of such sand spillover processes (Armishaw et al., 2000). Although the exact nature of such processes is not yet fully understood, it must be a combination or mixture of such processes that allows for the sorting and transfer of sands over such an extensive shelf-slope system.

5.3 Ancient analogues

Mixed process depositional systems have been described from Miocene and Early Pleistocene deep-sea sediments exposed on land in central Japan (Stow et al., 1998, 2002d; Ito, 1996, 1997, 2002). These show turbidites and other downslope facies interbedded with contourites and hemipelagites. The contourites were provisionally linked to deposition beneath an ancestral Kuroshio Current, although it was acknowledged at the time of publication that the origin of the bottom current forming these deposits remained controversial (Stow et al., 1998; Lee and Ogawa, 1998).

Several other ancient examples of contourite sand sheets in which a mix of

processes is evident have also been described. The Rifian Corridor in Morocco was the principal connection between the Mediterranean Sea and Atlantic Ocean during the late Miocene, prior to opening of the Gibraltar Gateway (Flecker et al., 2015). An extensive area (estimated > 500 km^2) along the northern margin of the Rifian seafloor, now exposed in central Morocco, was covered by a siliciclastic-dominant contourite sand sheet with ripples, large-scale dune cross-bedding, and sand ribbons (Capella et al., 2017). Individual sand bodies 5–50 m thick are encased in silty marl contourites and hemipelagites and associated with a moat and mounded contourite drift at the exit of the gateway. They formed in response to strong westward-directed bottom currents, probably modulated by deepwater tides at water depths of 150–400 m. Sediment was supplied both from upflow and from the gateway margins by mixed processes, including turbidity currents (Capella et al., 2017).

Across southern Cyprus, the late Oligocene to early Miocene carbonate-dominated succession is a classic example of a calci-contourite sedimentary system (Kahler and Stow, 1998; Stow et al., 2002e). Detailed study of the sediment facies and microfacies has identified a combination of downslope, alongslope and pelagic processes (Huneke et al., 2021) as well as an extensive sandy (calcarenite) contourite sheet, which is estimated to cover an area of at least 1000 km^2 with a thickness in excess of 5 m in places (Hernandez-Molina et al., 2018). Regional hiatuses are evident both below and above the sand sheet and are interpreted as the result of a strong bottom-current system active through the closing Tethys Ocean (Kahler and Stow, 1998).

Subsurface hydrocarbon exploration has highlighted further examples where presumed contourite sand sheets have been fed by downslope processes (turbidity currents) and then molded by alongslope currents. Good case studies are known from the Campos Basin slope offshore Brazil, of both Miocene (Viana et al., 2007) and Oligocene age (Mutti et al., 2015).

6. Conclusions

This study of oceanographic conditions, seafloor morphology and sediments around the central Ryukyu Islands has led to several important conclusions, which we suggest are significant for contourite research in general.

- We have identified a new area of contourite-controlled sedimentation in the NW Pacific Ocean and call this the *Ryukyu Sand Sheet*. This is one of the largest contourite sand sheets yet recognised, with an area of around 35,000 km^2, comprising mainly fine-grained sands, with current ripples and large-scale sediment waves.
- This sand sheet is being deposited under the influence of three principal current systems – the Kuroshio Current, the Kuroshio Countercurrent and the Ryukyu Current. The interaction of these currents with each other and with a complex seafloor and island-basin topography, leads to the development of meso-scale gyres, eddies and vortices. The high energy kinetics of the system result in winnowing and deposition of an extensive sandy substrate, with some gravels and locally exposed seafloor.
- We have demonstrated the significance of major wind-driven surface currents, as well as bottom currents associated with thermohaline circulation, in the deposition of sandy contourites that extend from shelf depths to over 1500 m water depth. The role of the modern Kuroshio Current in this context supports earlier work that proposed an ancestral Kuroshio Current for the deposition of Miocene contourites onshore Japan.
- The supply of sandy sediment to the Ryukyu Sand Sheet is by a process of seafloor polishing and sand spillover that involves combined oceanographic and gravitational processes. These winnow, remobilise and transport sediment off-shelf and downslope into the path of high-energy bottom currents.

Acknowledgements

We thank Ken Ikehara, Kohsaku Arai, Naotomo Kaneko, Kenji M. Matsuzaki, and Taku Ajioka for valuable discussions. We are also grateful to Kaiyo Engineering Co., Ltd., the crews of R/V *Kaiyomaru* No. 3 and No. 7 and R/V *Hakurei* for their professional help with the collections of samples and data. DS and UN thank Heriot-Watt University, Edinburgh, for general research support. The early versions of the manuscript received the benefit of many constructive comments by Francisco J. Rodríguez-Tovar, Amando Lasabuda, and the Editor Michele Rebesco.

Data Availability

The principal data and results are lodged with the Geological Survey of Japan in their Preliminary Research Reports series. These include: multibeam echosounder data, sub-bottom profiles, and sub-core samples and analytical results. Full bibliographic references in Itaki et al. (2010, 2011), Itaki (2015, 2018), Amano et al. (2013, 2015), and Nishida et al. (2016) (see below). All data are also available from the corresponding author on reasonable request.

References

Allen, J.R.L., 1982. Sedimentary Structures: Their Structure and Physical Basis, Volume 1. Amsterdam, The Netherlands, Elsevier, 593p.

Amano, A., Harigane, Y., Itaki, T., Arai, K., Matsumoto, D., Suzuki, A., Nakae, S., 2013. Bottom sediments around Yoron and Okinoerabu islands. In Arai, K. (Ed.), Marine geological and geophysical studies around Okinawa Island –around Okinoerabu-jima Island– Preliminary reports on researches in the 2012 fiscal year, GSJ Interim Report 61, 85–98 (in Japanese).

Amano, A., Itaki, T., Nishida, N., Katayama, H., Kaneko, N., Suzuki, A., Matsuzaki, K., 2015. Bottom sediments around Okinoerabu and Tokuno-shima islands. In: Itaki, T. (Ed.), Marine Geological and Geophysical Studies around Okinawa Island –around of Amami-oshima, Tokunoshima and Okinoerabu-jima Islands– Preliminary reports on researches in fiscal year 2014, GSJ Interim Report 67, 75–81 (in Japanese).

Armishaw, J.E., Holmes, R., Stow, D.A.V., 1998. Hebrides slope apron and Barra fan, NW UK continental margin sedimentation. Geol. Soc. Spec. Pub. 129, 81–104.

Armishaw, J.E., Holmes, R., Stow, D.A.V., 2000. The Barra Fan: A bottom-current reworked, glacially-fed submarine fan system. Mar. Petrol. Geol. 17, 219–239.

Brackenridge R.E., Nicholson, U., Stow D.A.V., Sapiie, B., Tappin, D.R., 2020. Indonesian throughflow as a preconditioning mechanism for submarine slides in the Makassar Strait. Geol. Soc. Spec. Pub. 500, 195–217.

609 Brackenridge, R.E., Stow, D.A.V., Hernández-Molina, F.J. , Jones, C., Mena, A., Alejo, I.,
610 Ducassou, E., Llave, E., Ercilla, G., Nombela, M.A., Perez-Arlucea, M., Frances, G.,
611 2018. Textural characteristics and facies of sand-rich contourite depositional
612 systems. Sedimentology 65, 2223–2252.
613 Broecker, W.S., 1991. The great ocean conveyor. Oceanogr. 4, 79–89.
614 Capella, W., Hernández-Molina, F.J., Flecker, R., Hilgen, F.J., Hssain, M., Kouwenhoven,
615 T.J., van Oorschot, M., Sierro, F.J., Stow, D.A.V., Trabucho-Alexandre, J., Tulbure,
616 M.A., de Weger, W., Yousfi, M.Z., Krijgsman, W., 2017. Sandy contourite drift in the
617 late Miocene Rifian Corridor (Morocco): Reconstruction of depositional
618 environments in a foreland-basin seaway. Sediment. Geol. 355, 31–57.Chen, H.,
619 Stow, D.A.V., Xie, X., Ren, J., Mao, K., Gao, Y., Chen, B., Zhang, W., Vandorpe T., Van
620 Rooij, D., 2021. Depositional architecture and evolution of basin-floor fan systems
621 since the Late Miocene in the Northwest Sub-Basin, South China Sea. Mar. Petrol.
622 Geol. 126, 1–22.
623 Chen, H., Xie, X., Zhang, W., Shu Y., Wang, D., Vandorpe, T., Van Rooij, D., 2016. Deep-
624 water sedimentary systems and their relationship with bottom currents at the
625 intersection of Xisha Trough and Northwest Sub-Basin, South China Sea. Mar. Geol.
626 378, 101–113.
627 Crameri, F., 2018. Scientific colour maps. Zenodo.
628 http://doi.org/10.5281/zenodo.1243862
629 Dalrymple, R.W., LeGresley, E.M., Fader, G.B.J., Petrie, B.D., 1992. The western Grand
630 Banks of Newfoundland: Transgressive Holocene sedimentation under the
631 combined influence of waves and currents. Mar. Geol. 105, 95–118.
632 Das, P., Lin, A.T.S., Chen, M.P.P., Miramontes, E., Liu, C.S., Huang, N.W., Kung, J., Hsu,
633 S.K., Pillutla, R.K., Nayak, K., 2021. Deep-sea submarine erosion by the Kuroshio
634 Current in the Manila accretionary prism, offshore Southern Taiwan.
635 Tectonophysics 807, 228813.
636 Davies, S., Stow, D.A.V., Nicholson, U., 2021. Late Glacial to Holocene Sedimentary
637 Facies of the Eirik Drift, Southern Greenland Margin: Spatial and Temporal
638 Variability and Paleoceanographic Implications. Mar. Geol. 440, 1–19.
639 Faugères, J.-C., Mezerais, M.L., Stow, D.A.V., 1993. Contourite drift types and their
640 distribution in the North and South Atlantic Ocean basins. Sediment. Geol. 82, 189–
641 203.
642 Faugères, J.-C., Stow, D.A.V., 2008. Contourite drifts: nature, evolution and controls. In:
643 Rebesco, M., Camerlenghi, A. (Eds.), Contourites. Developments in Sedimentology
644 Series, Elsevier, 60, 259–288.
645 Faugères, J.-C., Stow, D.A.V., Imbert, P., Viana, A., 1999. Seismic features diagnostic of

646 contourite drifts. Mar. Geol. 162, 1–38.
647 Flecker, R., Krijgsman, W., Capella, W., de Castro Martíns, C., Dmitrieva, E., Mayser,
648 J.P., Marzocchi, A., Modestou, S., Ochoa, D., Simon, D., Tulbure, M., van den Berg,
649 B., van der Schee, M., de Lange, G., Ellam, R., Govers, R., Gutjahr, M., Hilgen, F.,
650 Kouwenhoven, T., Lofi, J., Meijer, P., Sierro, F.J., Bachiri, N., Barhoun, N., Alami,
651 A.C., Chacon, B., Flores, J.A., Gregory, J., Howard, J., Lunt, D., Ochoa, M., Pancost,
652 R.,Vincent, S., Yousfi, M.Z., 2015. Evolution of the Late Miocene Mediterranean–
653 Atlantic gateways and their impact on regional and global environmental change.
654 Ear.-Sci. Rev. 150, 365–392.
655 Flemming, B.W., 1980. Sand transport and bedform patterns on the continental shelf
656 between Durban and Port Elizabeth (southeast African continental margin).
657 Sediment. Geol. 26, 179–205.
658 Gardner, W.D., Richardson, M.J., Cacchione, D.A., 1989. Sedimentological effects of
659 strong southward flow in the Straits of Florida. Mar. Geol. 86, 155–180.
660 Gardner, W.D., Tucholke, B.E., Richardson, M.J. Biscaye, P.E., 2017. Benthic storms,
661 nepheloid layers, and linkage with upper ocean dynamics in the western North
662 Atlantic. Mar. Geol. 385, 304–327.
663 Hernández-Molina, J., Hodell, D.A., Stow, D.A.V., Alvarez-Zarikian, C.A. (Eds.), 2016.
664 Stratigraphic and Sedimentary Significance of the Mediterranean Outflow Water
665 and its Conceptual Implications. Mar. Geol. Sp. Iss., 377, 150pp.
666 Hernández-Molina, F.J., Huneke, H., Rodriguez-Tovar, F.J., Llave, E., Ng, Z.L., Chiarella,
667 D., Suklap, S., Docherty, B., Mena, A., Stow, D.A.V., 2018. Deep-water bottom
668 current deposits from Cyprus: an ancient analogue for contourite terraces and
669 plastered drifts? 20th Int. Sedimentological Congress, 13–17 August 2018. Quebec,
670 Canada. Abstracts.
671 Hernández-Molina, F.J., Llave, E., Stow, D.A.V., 2008a. Continental slope contourites.
672 In: Rebesco, M., Camerlenghi, A. (Eds.), Contourites. Developments in
673 Sedimentology Series, Elsevier, 60, 379–400.
674 Hernández-Molina, F.J., Stow, D.A.V., Alvarez-Zarikian, C.A., Acton, G., Bahr, A.,
675 Balestra, B., Ducassou, E., Flood, R., Flores, J.-H., Furota, S., Grunert, G., Hodell, D.,
676 Jimenez-Espejo, F., Kim, J.K., Krissek, L., Kuroda, J., Li, B., Llave, E., Lofi, J., Lourens,
677 L., Miller, M., Nanayama, F., Nishida, N., Richter, C., Roque, C., Pereira H., Sanchez
678 Goñi, M.F., Sierro, F.J., Singh, A.D., Sloss, C., Takashimizu, Y., Tzanova, A., Voelker,

679 A., Williams, T., Xuan Chang, 2014. Onset of Mediterranean Outflow into the North
680 Atlantic. Science 344, 1244–1250.
681 Hernández-Molina, F.J., Stow, D.A.V., Maldonado, A. 2008b. Abyssal plain contourites.
682 In: Rebesco, M., Camerlenghi, A. (Eds.), Contourites. Developments in
683 Sedimentology Series, Elsevier, 60, 347–378.
684 Holloway, G., 1992. Representing topographic stress for large-scale ocean models. J.
685 Phys. Oceanogr. 22, 1033–1046.
686 Howe, J.A.,Stocker, M.S., Stow, D.A.V., 1994. Late Cenozoic sediment drift complex,
687 northeast Rockall Trough, North Atlantic. Paleoceanography 9, 989–1000.
688 Hsin, Y.C., Wu, C.R., Shaw, P.T., 2008. Spatial and temporal variations of the Kuroshio
689 east of Taiwan, 1982–2005: A numerical study. J. Geophys. Res.: Oceans 113,
690 C04002, doi:10.1029/2007JC004485.
691 Hsu, P.C., Chang, M.H., Lin, C.C., Huang, S.J., Ho, C.R., 2017. Investigation of the island-
692 induced ocean vortex train of the Kuroshio Current using satellite imagery. Remote
693 Sensing of Environment 193, 54–64.
694 Hüneke H, Hernández-Molina FJ, Rodríguez-Tovar FJ, Llave E, Chiarella D, Mena A,
695 Stow D.A.V., 2021. Diagnostic criteria for calcareous contourites, turbidites and
696 pelagites in the Eocene–Miocene slope succession, southern Cyprus.
697 Sedimentology 68, 557–592
698 Ikehara, K., Kinoshita, Y., 1994. Distribution and origin of subaqueous dunes on the
699 shelf of Japan. Sediment. Geol. 120, 75–87.
700 Itaki, T., 2015. Sedimentological Map of the Vicinity of Northern Okinawa-Jima Island:
701 Marine Geology Map Series, no. 85 (DVD), Geological Survey of Japan, AIST.
702 Itaki, T., 2018. Sedimentological Map of the Vicinity of Southern Okinawa-Jima Island:
703 Marine Geology Map Series, no. 90 (DVD), Geological Survey of Japan, AIST.
704 Itaki, T., Amano, A., Katayama, H., Suzuki, A., Kaneko, N., Nishida, N., Shimamura, M.,
705 Lee, S., Arai, K., 2011. Bottom sediments in west off the Okinawa main island
706 (around Kume-Zima and Kerama islands). In: Arai, K. (Ed.), Marine geological and
707 geophysical studies around Okinawa Island –western off of Okinawa Island–
708 Preliminary reports on researches in the 2010 fiscal year, GSJ Interim Report 55,
709 57–67 (in Japanese).
710 Itaki, T., Katayama, H., Suzuki, A., Kaneko, N., Oda, H., Arai, K., 2010. Bottom sediments
711 in west off the Okinawa main island. In: Arai, K. (Ed.), Marine geological and

712 geophysical studies around Okinawa Island –northwestern off of Okinawa Island–
713 Preliminary reports on researches in the 2009 fiscal year, GSJ Interim Report 51,
714 54–68 (in Japanese).
715 Ito, M., 1996. Sandy contourites of the lower Kazusa Group in the Boso Peninsula,
716 Japan; Kuroshio-current-influenced deep-sea sedimentation in a Plio-Pleistocene
717 forearc basin. J. Sediment. Res. 66, 587–598.
718 Ito, M., 1997. Spatial variation in turbidite-to-contourite continuums of the Kiwada and
719 Otadai formations in the Boso Peninsula, Japan; an unstable bottom-current
720 system in a Plio-Pleistocene forearc basin. J. Sediment. Res. 67, 571–582.
721 Ito, M., 2002. Kuroshio current-influenced sandy contourites from the Plio-Pleistocene
722 Kazusa forearc basin, Boso Peninsula, Japan. In: Stow, D.A.V., Pudsey, C.J., Howe,
723 J.A., Faugères, J.-C., Viana, A.R. (Eds.), Deep-water Contourite Systems: Modern
724 Drifts and Ancient Series, Seismic and Sedimentary Characteristics: Geol. Soc.
725 London Mem. 22, 421–432.
726 Kahler, G., Stow, D.A.V., 1998. Turbidites and contourites of the Paleogene Lefkara
727 Formation, S. Cyprus. Sediment. Geol. 115, 215–232.
728 Kamidaira, Y., Uchiyama, Y., Mitarai, S., 2017. Eddy-induced transport of the Kuroshio
729 warm water around the Ryukyu Islands in the East China Sea. Conti. Shelf Res. 143,
730 206–218.
731 Kawabe, M., 1995. Variation of current path, velocity, and volume transport of the
732 Kuroshio in relation with the large meander. J. Phys. Oceanogr. 25, 3103–3117.
733 Knutz, P., 2008. Palaeoceanographic significance of contourite drifts. In: M Rebesco, A
734 Camerlenghi (editors), *Contourites*, Developments in Sedimentology Series,
735 Elsevier, 60, 511–535.
736 Konda, M., Ichikawa, H., Han, I.S., Zhu, X.H., Ichikawa, K., 2005. Variability of current
737 structure due to meso-scale eddies on the bottom slope southeast of Okinawa
738 Island. J. Oceanogr. 61, 1089–1099.
739 Kubo, Y., Soh, W., Machiyama, H., Tokuyama, H., 2004. Bedforms produced by the
740 Kuroshio Current passing over the northern Izu Ridge. Geo-Mar. Lett. 24, 1–7.
741 Laberg, J.S., Camerlenghi, A., 2008. The significance of contourites for submarine slope
742 stability. In: M Rebesco, A Camerlenghi (editors), *Contourites*, Developments in
743 Sedimentology Series, Elsevier, 60, 537–556.
744 Lasabuda, A., Geissler, W. H., Laberg, J. S., Knutsen, S.-M., Rydningen, T. A., Berglar, K.,

745 2018. Late Cenozoic erosion estimates for the northern Barents Sea: Quantifying
746 glacial sediment input to the Arctic Ocean. Geochemistry, Geophysics, Geosystems,
747 19, 4876–4903.
748 Lee, I.T., Ogawa, Y., 1998. Bottom-current deposits in the Miocene–Pliocene Misaki
749 Formation, Izu forearc area, Japan. Island Arc 7, 315–329.
750 Lie, H.-J., Cho, C.-H., Kaneko, A., 1998. On the branching of the Kuroshio and the
751 formation of slope countercurrent in the East China Sea: Proceedings of Japan-
752 China Joint Symposium on Cooperative Study of Subtropical Circulation System,
753 25–41.
754 Lonsdale. P., 1981. Drifts and ponds of reworked pelagic sediment in part of the
755 Southwest Pacific. Mar. Geol. 43, 153–193.
756 Lonsdale, P., Malfait, PI., 1974. Abyssal dunes of foraminiferal sand in Carnegie Ridge.
757 Geol. Soc. Am. Bull. 85, 1679–1712.
758 Lonsdale, P., Normark, W.R., Neuman, W.A., 1972. Sedimentation and erosion on
759 Horizon Guyot. Geol. Soc. Am. Bull. 83, 289–316.
760 Mulder, T., Faugères, J.C., Gonthier, E., 2008. Mixed turbidite-contourite systems. In:
761 M Rebesco, A Camerlenghi (editors), *Contourites*, Developments in Sedimentology
762 Series, Elsevier, 60, 435–456.
763 Mutti, E., Cunha, R.S., Bulhoes, E.M., Arienti, L.M., Viana, A.R., 2015. Contourites and
764 Turbidites of the Brazilian Marginal Basins. Search and Discovery Article #51069,
765 Adapted from oral presentation at AAPG Annual Convention & Exhibition,
766 Houston, USA, April 6–9, 2014.
767 Nagao, M., Furushima, Y. Suzuki, A., 2011. Shipboard acoustic current profiling of GH10
768 cruise (Southwest of Okinawa island). In: Arai, K. (Ed.), Marine Geological and
769 Geophysical Studies around Okinawa Island –western off of Okinawa Island–
770 Preliminary Reports on Researches in the 2010 Fiscal Year, GSJ Interim Report. 55,
771 42–49 (in Japanese).
772 Nakamura, H., Nishina, A., Ichikawa, H., Nonaka, M. Sasaki, H., 2008. Deep
773 countercurrent beneath the Kuroshio in the Okinawa Trough. J. Geophys. Res. 113,
774 C06030, doi:10.1029/2007JC004574.
775 Nakamura, H., Nishina, A., Liu, J., Tanaka, F., Wimbush, M., Park, J-H., 2013.
776 Intermediate and deep water formation in the Okinawa Trough. Jour. Geophys.
777 Res. Oceans 118, 6881–6893.

778 Nicholson, U., Libby, S., Tappin, D.R., McCarthy, D., 2020. The Subantarctic Front as a
779 sedimentary conveyor belt for tsunamigenic submarine landslides. Mar. Geol. 424,
780 106161.
781 Nicholson, U., Stow, D., 2019. Erosion and deposition beneath the Subantarctic Front
782 since the Early Oligocene. Sci. Rep. 9, 1–9.
783 Nishida, N., Ajioka, T., Ikehara, K., Nakashima, R., Katayama, H., Sato, T., Furuyama, S.,
784 Tamura, T., 2020. Postglacial stratigraphic evolution of a current-influenced sandy
785 shelf: Offshore Kujukuri strandplain, central Japan. Sedimentology 67, 559–575.
786 Nishida, N., Ikehara, K., 2013. Holocene evolution of depositional processes off
787 southwest Japan: Response to the Tsushima Warm Current and sea-level rise.
788 Sediment. Geol., 290, 138–148.
789 Nishida, N., Itaki, T., Katayama, H., Kaneko, N., Ajioka, T., Amano, A., Hiramoto, J.,
790 2016. Sea-floor sediments around Amami Ohshima, Tokunoshima, and Kikaijima
791 islands. In: Itaki, T. (Ed.), Marine Geological and geophysical studies around
792 Okinawa Island –aroud Amami-Oshima Islands– Preliminary reports on researches
793 in the 2015 fiscal year, GSJ Interim Report, 70, 66–74 (in Japanese).
794 Ohta, A., Imai, N., Tachibana, Y., Amano, A., Itaki, T., Arai, K., Ikehara, K., Okai, T., 2013.
795 Chemical composition of marine sediments around Okinoerabu Island, Japan. In:
796 Arai, K. (Ed.), Marine geological and geophysical studies around Okinawa Island –
797 aroud Okinoerabu-jima Island– Preliminary reports on researches in the 2012 fiscal
798 year, GSJ Interim Report 61, 99–107 (in Japanese).
799 Ohta, A., Imai, N., Tachibana, Y., Amano, A., Itaki, T., Katayama, H., Okai, T., 2016.
800 Chemical composition of marine surface in the northwest of Okinoerabujima and
801 Tokunoshima (GK14 Cruise), Japan. In: Itaki, T. (Ed.), Marine geological and
802 geophysical studies around Okinawa Islands –aroud of Amami-oshima Island–
803 Preliminary reports on researches in the 2015 fiscal year, GSJ Interim Report 70,
804 88–98 (in Japanese).
805 Palamenghi, L., Keil, H., Spiess, V., 2015. Sequence stratigraphic framework of a mixed
806 turbidite-contourite depositional system along the NW slope of the South China
807 Sea. Geo-Mar. Lett. 25, 1–21.
808 Preu, B., Spiess, V., Schwenk, T., Sneider, R., 2011. Evidence for current-controlled
809 sedimentation along the southern Mozambique continental margin since Early
810 Miocene times. Geo-Mar. Lett. 31, 427–435.

Ramsay, P.J., 1994. Marine geology of the Sodwana Bay shelf, southeast Africa. Mar. Geol. 120, 225–247.

Rebesco, M., 2005. Contourites. In: Selley, R.C. et al., (editors), Encyclopedia of Geology, Elsevier, Oxford, 4, 513–527.

Rebesco, M., Camerlenghi, A. (Eds.), 2008. Contourites. Developments in Sedimentology Series, Elsevier, 60.

Rebesco, M., Camerlenghi, A., Munari, V., Mosetti, R., Ford, J., Micallef, A., Facchin, L., 2021. Bottom current-controlled Quaternary sedimentation at the foot of the Malta Escarpment (Ionian Basin, Mediterranean). Mar. Geol. 441, 106596.

Rebesco, M., Hernández-Molina, F.J., Van Rooij, D., Wahlin, A., 2014. Contourites and associated sediments controlled by deep-water circulation processes: State-of-the-art and future considerations. Mar. Geol. 352, 111–154.

Schlitzer, R. 2020. Ocean Data View, ODV 5.2.1, http://odv.awi.de

Sheen, K.L., White, N.J., Caulfield, C.P., Hobbs, R.W., 2012. Seismic imaging of a large horizontal vortex at abyssal depths beneath the Sub-Antarctic Front. Nat. Geosci. 5, 542–546.

Smillie, Z., Stow, D.A.V., Esentia, I., 2018. Contourite drifts, erosional features and bedforms. In: Cochran, J. Kirk; Bokuniewicz, J. Henry; Yager, L. Patricia (Eds.) Encyclopedia of Ocean Sciences, 3rd Edition 4, 97–110, Elsevier.

Stow, D.A.V., Armishaw, J.E., Holmes, R., 2002c. Holocene contourite sand sheet on the Barra Fan slope, NW Hebridean margin. Geol. Soc. London. Mem. 22, 99–120.

Stow, D.A.V., Faugères, J.-C., (Eds.), 1993. Contourites and Bottom Currents. Sediment. Geol. Sp. Vol. 82, 310pp.

Stow, D.A.V., Faugères, J.-C., (Eds.), 1998. Contourites, Turbidites and Process Interaction, Sediment. Geol. Sp. Is. 115, Nos. 1–4, 386pp.

Stow, D.A.V., Faugères, J.-C., 2008. Contourite facies and the facies model. In: Rebesco, M., Camerlenghi, A. (Eds.), Contourites. Developments in Sedimentology 60. Elsevier, Amsterdam, 223–256.

Stow, D.A.V., Hernández-Molina, F.J., Alvarez Zarikian, C.A., the Expedition 339 Scientists, 2013a. Proc. IODP, 339: Tokyo (Integrated Ocean Drilling Program Management International, Inc.).

Stow, D.A.V., Hernández-Molina, F.J., Llave, E., Bruno, M., García M, Díaz del Rio, V., Somoza, L., Brackenridge, R.E., 2013b. The Cadiz Contourite Channel: sandy

844 contourites, bedforms and dynamic current interaction. Mar. Geol. 343, 99–114.
845 Stow, D.A.V., Hernández-Molina, F.J., Llave, E., Sayago-Gil, M., Díaz del Río, V. Branson,
846 A, 2009. Bedform-velocity matrix: The estimation of bottom current velocity from
847 bedform observations. Geology 37, 327–330.
848 Stow, D.A.V., Holbrook, J.A., 1984. Hatton Drift contourites, Northeast Atlantic, Deep
849 Sea Drilling Project Leg 81. Init. Rep. DSDP 81, 695–699.
850 Stow, D.A.V., Kahler, G., Reeder, M., 2002e. Fossil contourites: type example from an
851 Oligocene paleoslope system, Cyprus. Geol. Soc. London. Memoir 22, 443–456.
852 Stow, D.A.V., Mayall, M., 2000. Deep-water Sedimentary Systems: New Models for the
853 21st Century. Mar. Petrol. Geol. 17, 125–136.
854 Stow, D.A.V., Ogawa, Y., Lee, I.T., Mitsuzawa, K., 2002d. Neogene contourites, Miura-
855 Boso forearc basin, SE Japan. Geol. Soc. London. Mem. 22, 409–420.
856 Stow, D.A.V., Pudsey, C.J., Howe, J.A., Faugères, J.C., Viana, A., (Eds.), 2002a. Atlas of
857 deep-water contourite systems: modern drifts and ancient series, seismic and
858 sedimentary characteristics. An IGCP 432 publication, Geol. Soc. London. Mem. 22,
859 464pp.
860 Stow, D.A.V., Pudsey, C.J., Howe, J.A., Faugères, J.C., Viana, A. 2002b. Bottom currents
861 and contourites: state-of-the-art. Geol. Soc. London. Mem. 22, 7–20.
862 Stow, D.A.V., Smillie, Z., 2020. Distinguishing between deepwater sediment facies:
863 turbidites, contourites and hemipelagites. Geosciences 10, 68.
864 Stow, D.A.V., Smillie Z., Pan J., Esentia I., 2018. Deep-sea contourites: sediments and
865 cycles. In: Cochran, J. Kirk; Bokuniewicz, J. Henry; Yager, L. Patricia (Eds.)
866 Encyclopedia of Ocean Sciences, 3rd Edition. vol. 4, pp. 111-120, Elsevier.
867 Stow, D.A.V., Taira, A., Ogawa, Y., Soh, W., Taniguchi, H., Pickering, K.T., 1998.
868 Volcaniclastic sediments, process interaction and depositional setting of the
869 Miocene-Pliocene Miura Group, SE Japan. Sediment. Geol. 115, 351–382.
870 Taft, B.A., 1978. Structure of Kuroshio south of Japan. J. Mar. Res. 36, 77–117.
871 Talley, L.D., 2013. Closure of the Global Overturning Circulation Through the Indian,
872 Pacific, and Southern Oceans: Schematics and transports. Oceanogr. 26, 80–97.
873 Talley, L.D., Pickard, G.L., Emery, W.J., Swift, J.H., 2011. Descriptive Physical
874 Oceanography (Sixth edition), Elsevier, London, 560p.
875 Thoppil, P.G., Metzger, E.J., Hurlburt, H.E., Smedstad, O.M., Ichikawa, H., 2016. The
876 current system east of the Ryukyu Islands as revealed by a global ocean reanalysis.

877 Prog. Oceanogr. 141, 239–258.
878 Tsuji, Y., 1993. Tide influenced high energy environments and rhodolith-associated
879 carbonate deposition on the outer shelf and slope off the Miyako Islands, southern
880 Ryukyu Island Arc, Japan. Mar. Geol. 113, 255–271.
881 Verdicchio, G., Trincardi, F., 2008. Shallow-water contourites. In: Rebesco, M.,
882 Camerlenghi, A. (Eds.), Contourites. Developments in Sedimentology 60. Elsevier,
883 Amsterdam, 409–434.
884 Viana, A.R., Almeida, W., Nunes, M.C.V., Bulhoes, E.M., 2007. The economic
885 importance of contourites. Geol. Soc. London. Spec. Pub. 276, 1–24.
886 Viana, A.R., Faugères, J.-C., Stow, D.A.V., 1998. Bottom-current controlled sand
887 deposits: a review from modern shallow to deep water environments. Sediment.
888 Geol. 115, 53–80.
889 Viana, A.R., Hercos, C., de Almeida, W., Magelhaes, J.L.C., de Andrade, S.B., 2002.
890 Evidence of bottom current influence on the Neogene to Quaternary sedimentation
891 along the northern Campos slope, SW Atlantic margin. Geol. Soc. London. Mem. 22,
892 249–260.
893 Viana, A.R., Rebesco, M., 2007. Economic and palaeoceanographic significance of
894 contourite deposits. Geol. Soc. London Spec. Pub. 350p.
895 Wei, Y., 2018. Cross-Shelf Circulation Induced by the Kuroshio Shear Stress in the East
896 China Sea. J. Phys. Oceanogr. 48, 1479–1793.
897 Wynn, R.W., Stow, D.A.V. editors. 2002. Recognition and interpretation of deep-water
898 sediment waves: implications for paleoceanography hydrocarbon exploration and
899 flow process interpretation. Mar. Geol. Spec. Iss. vol 192.
900 Zhang, Y., Zhang, Z., Chen, D., Qiu, B., Wang, W., 2020. Strengthening of the Kuroshio
901 current by intensifying tropical cyclones. Science 368, 988–993.
902 Zhao, Y., Liu, Z., 2017. Spatial distribution of contourites in the global ocean and its
903 paleoclimatic significance. Advances in Earth Science 32, 287–296.
904 Zhao, R., Nakamura, H., Zhu, X.-H., Park, J.-H., Nishina, A., Zhang, C., Na, H., Jeon, C.,
905 Zhu, Z.-N., Sik Min, H., 2020. Tempo-spatial variations of the Ryukyu Current
906 southeast of Miyakojima Island determined from mooring observations. Sci. Rep.
907 10, 6656.
908
909

FIGURE AND TABLE CAPTIONS

Figure 1. (A) Bathymetry map (contour interval of 1 km) showing the location of main current systems around the Ryukyu Islands of south-west Japan. The purple polygon shows the core of the Kuroshio Current, where average velocities exceed 50 cm/s; The green polygon shows the core of the Ryukyu Current, where average velocities exceed 10 cm/s at 500–700 m water depth (modified from Thoppil et al., 2016). Ryukyu Islands: Am – Amami-Oshima, Tk – Tokunoshima, Ok – Okinawa, Mi – Miyako, Ir – Iriomote, TS – Tokara Strait. Image produced using GeoMapApp. (B) Water masses and currents along a NW-SE transect across the Ryukyu Arc. Bathymetry and water temperature profile generated using Ocean Data aView (Schlitzer, 2020). Velocity contours are from Wei (2018) for the Kuroshio Current and Thoppil et al. (2016) for the Ryukyu Current. Positive values show flow to the NE, contour interval is 10 cm/s. (C) Eddy Kinetic Energy and (D) surface vorticity around the Ryukyu islands, January 2012 (modified from Kamidaira et al., 2017).

Figure 2. Map of the study area showing the distribution of surface sediments. Data are from Itaki et al. (2010, 2011), Itaki (2015, 2018), Amano et al. (2013, 2015), and Nishida et al. (2016). Current direction (arrows) and sense (bars) of ripples determined from seafloor photographs. The Ryukyu Sand Sheet extends at minimum over the coloured area covered with sand and gravel.

Figure 3. Sub-bottom profile images west of Tokunoshima Island (Tk), including a NE-SW profile (SBP1012b) and two NW-SE profiles (SBP40a and SBP41b). Depositional features include a plastered contourite drift and large-scale sediment waves.

Figure 4. Map showing the detailed seafloor topography obtained by using a multi-beam echo sounder around Amami-Oshima. Locations of figures 5–7 are highlighted.

Figure 5. (A) Bathymetry west of Tokunoshima Island (location shown in Figure 4), showing large-scale sediment waves oriented oblique to the slope on a drift deposit, at 700–900 m water depth in association with moats. (B and C) Sub-bottom profiles across the drift (see Figure 3 for full profiles) showing seabed morphology, including large-scale sediment waves with a moat.

941 Figure 6. Bathymetry east of Tokunoshima Island (location shown in Figure 4), where
942 the seabed is influenced by the Ryukyu Current. Large-scale sediment waves form
943 at 600–700 m water depth. They are oriented parallel-oblique to slope contours
944 and likely formed by a combination of down-slope and along-slope processes.

945 Figure 7. Bathymetry east of Amami-Oshima Island (location shown in Figure 4). Large-
946 scale sediment waves are oriented perpendicular to the slope at water depths of
947 700–950 m, with a concave-to-southwest morphology – possibly indicating
948 deposition under NE-flowing bottom currents. Large-scale bedforms also form
949 parallel to slope in the east of the map, exclusively in association with channels and
950 canyons – indicating deposition from sediment gravity flows in the canyons.
951 Oblique bedforms are also evident. Basinal areas display sheeted fill characterised
952 by a flat seabed.

953 Figure 8. Seafloor photographs, sandy substrate with regular to irregular, straight-
954 crested to linguoid ripples. A: Station 445, water depth 720 m; B: Station 831,
955 water depth 784 m; C: Station 862, water depth 389 m; D: Station 899, water
956 depth 472 m. The compass, used for scale, is 40 cm long. The colour variation
957 between A and others is due to the difference of the camera system.

958 Figure 9. Photographs of selected sub-core samples with matching x-radiograph
959 images, taken from same stations illustrated in Figure 8. Sand-rich facies with clear
960 parallel and cross lamination indicated by the white triangles. A: Well-sorted
961 foraminifera-rich medium sand. Bioturbation (B) is recognised in parts. Station 445,
962 water depth 720 m; B: Alternating beds of medium sand (ms) and fine sand (fs).
963 Station 831, water depth 784 m; C: Well-sorted fine sand. Station 862, water depth
964 389 m; D: Well-sorted medium sand with faint lamination. Station 899, water
965 depth 472 m.

966 Figure 10. Relationship between ripple wavelength, from crest to crest, and the
967 median grain size of ripples (*N* = 66 stations). The median grain size data are from
968 Itaki (2015). vfs: very fine sand; fs: fine sand; ms: medium sand; cs: coarse sand.

969 Table 1. Station information and ripple features observed at each station.

970 Table 2. Comparison of major sand sheet worldwide including the Ryukyu Sand Sheet.
971 It is highlighted that the Ryukyu Sand Sheet, which is formed by the mixed

processes influenced by the Kuroshio Current in the Northwestern Pacific, is one of the largest sand sheets worldwide.

Supplemental Figure 1. Map showing sampling locations with all station numbers.

Animation 1. ROV video showing an actively flowing bottom current and rippled sand at Station OK41 (405 m water depth).

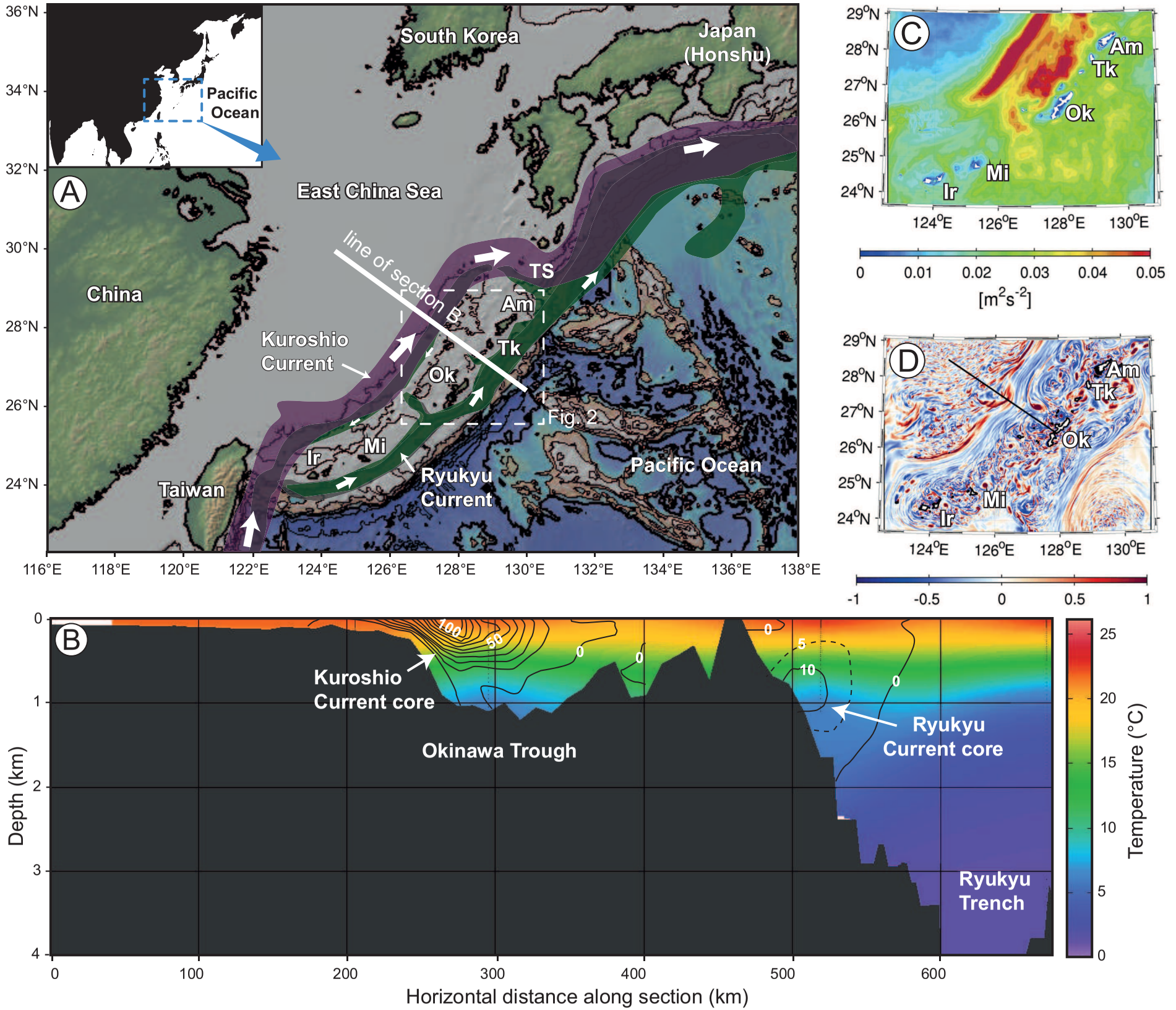

Figure 1

Click here to access/download;Figure;Fig. 1 Map and oceanography_r.eps

Figure 2

Click here to access/download;Figure;Fig. 2 Surface sediments_r.eps

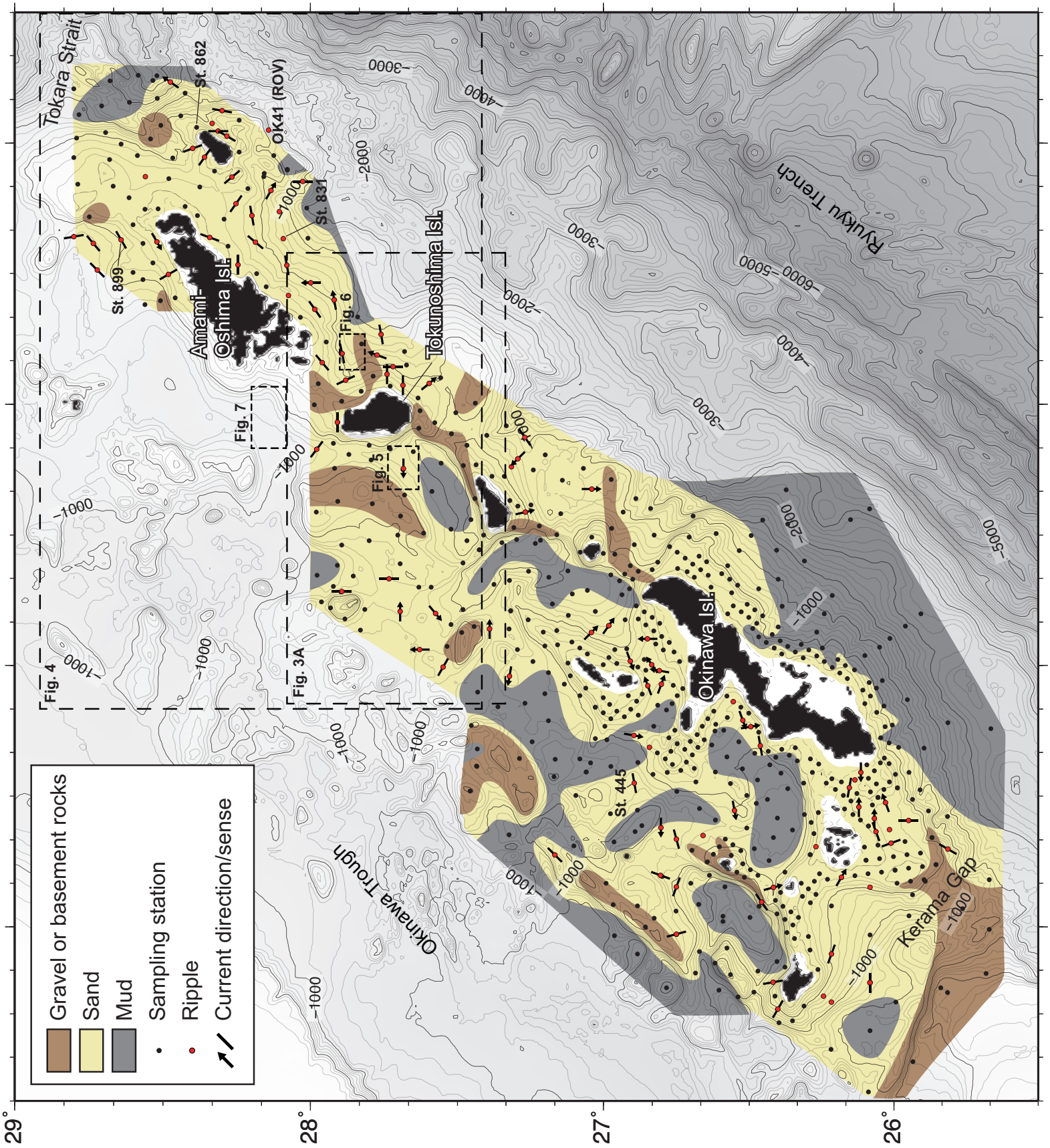

Figure 3

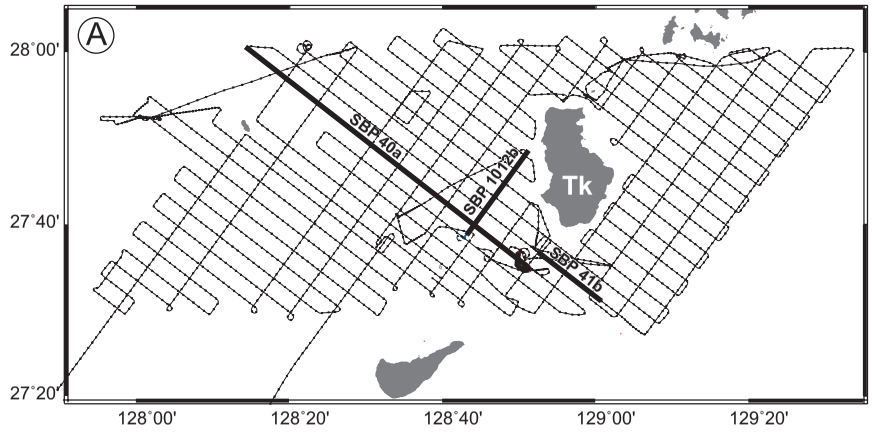

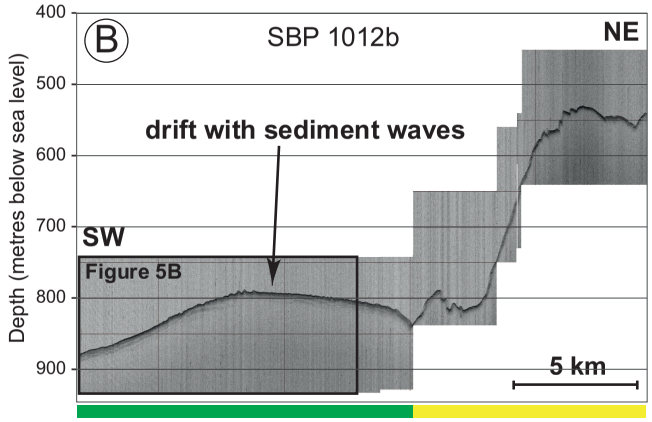

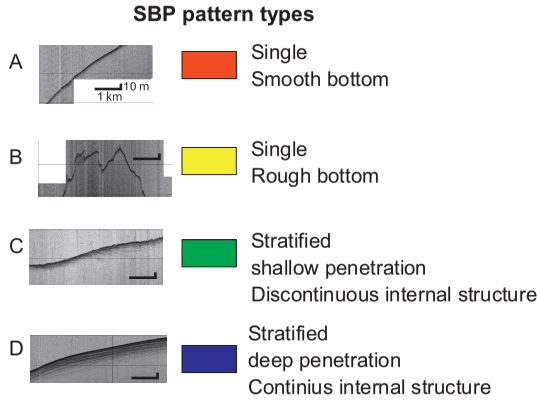

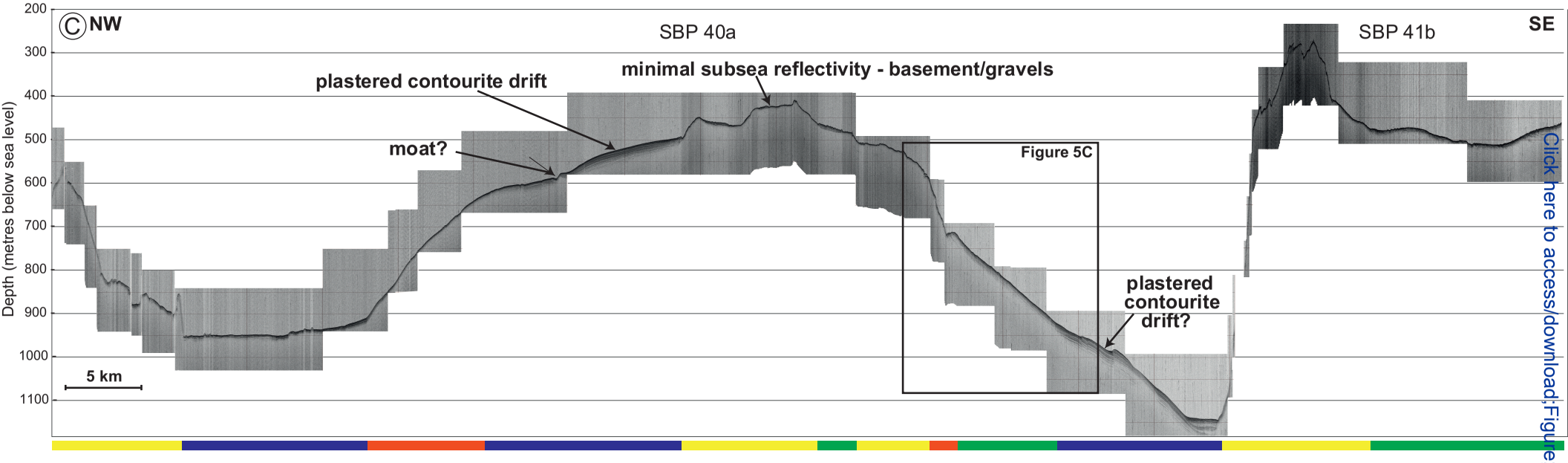

Figure 4

Click here to access/download:Figure:Fig. 4 Batymetry index_r2.eps

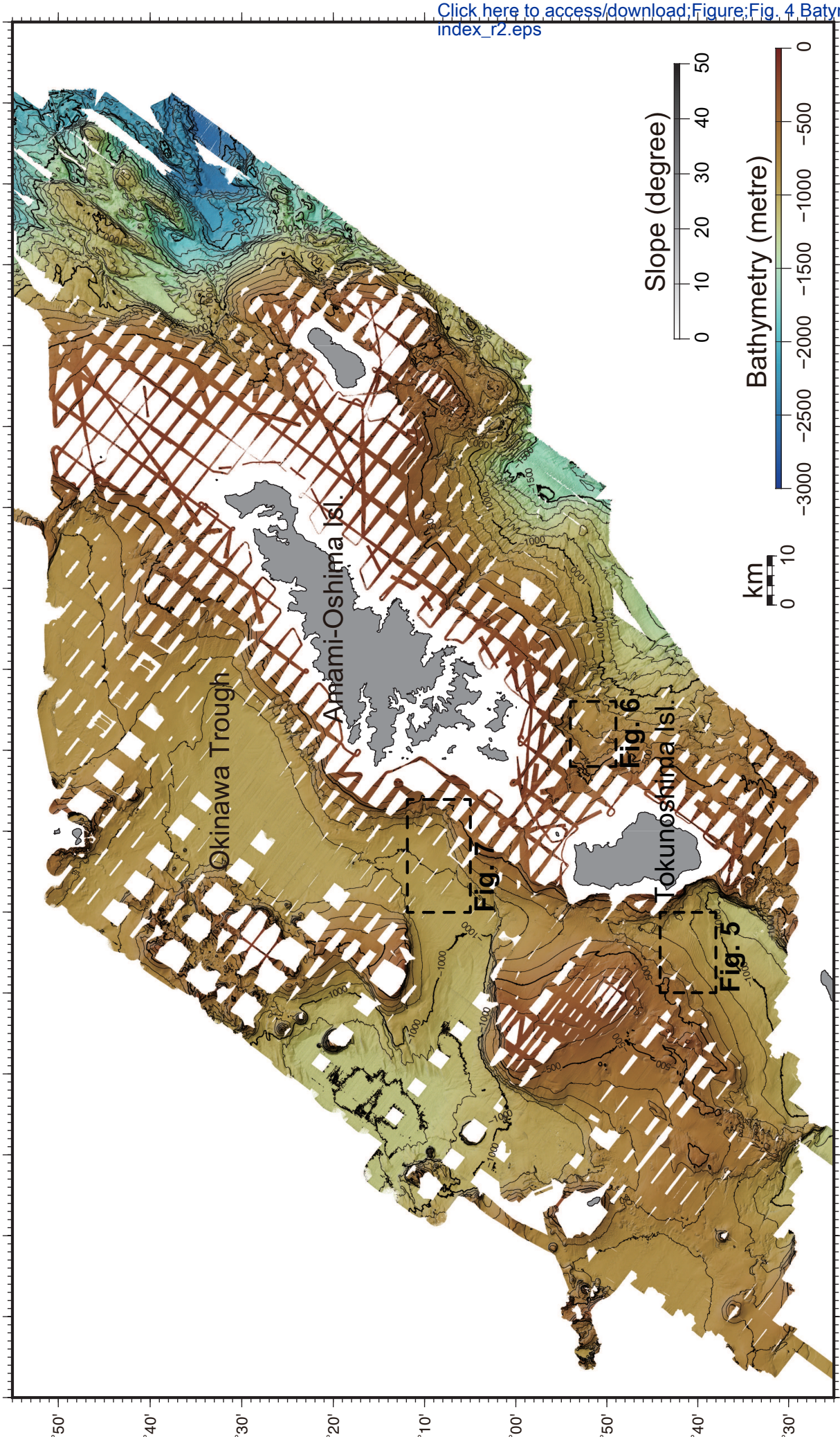

Figure 5

Click here to access/download;Figure;Fig. 5 SedWavs_along slope_r.eps

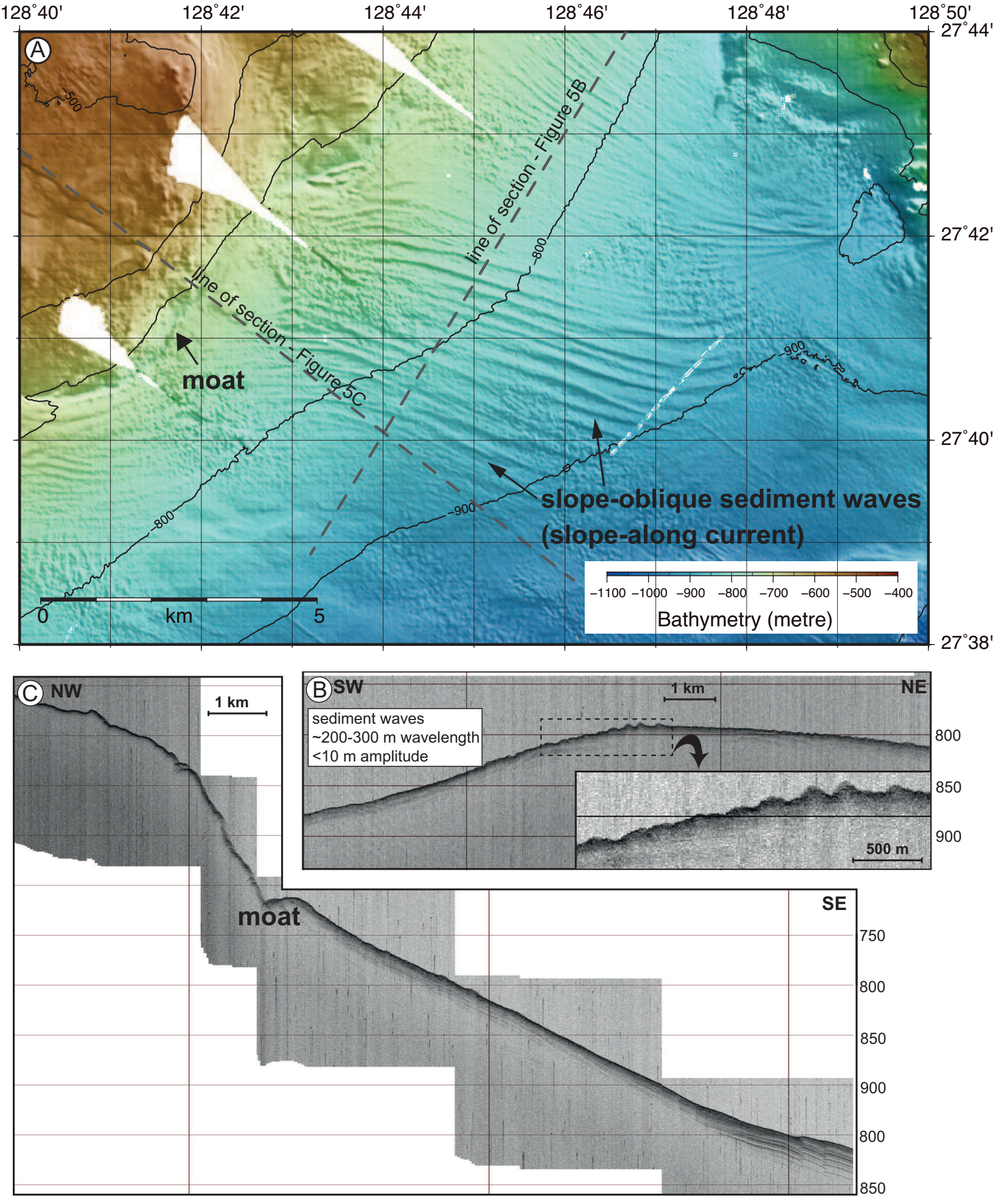

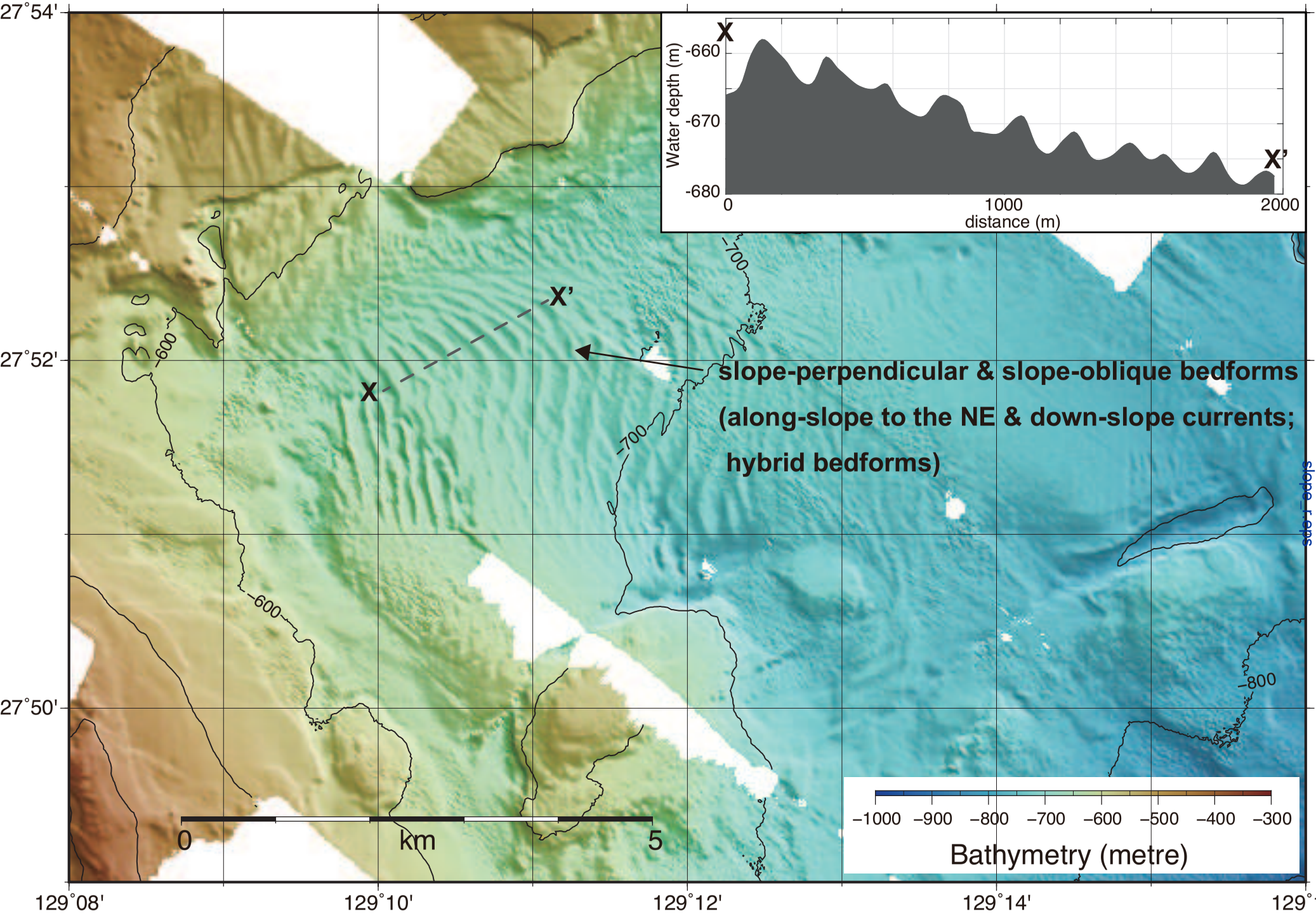

Figure 6

Click here to access/download;Figure;Fig. 6 SedWavs_down slope_r.eps

Figure 7

Click here to access/download;Figure;Fig. 7 SedWavs_mixed processes_r.eps

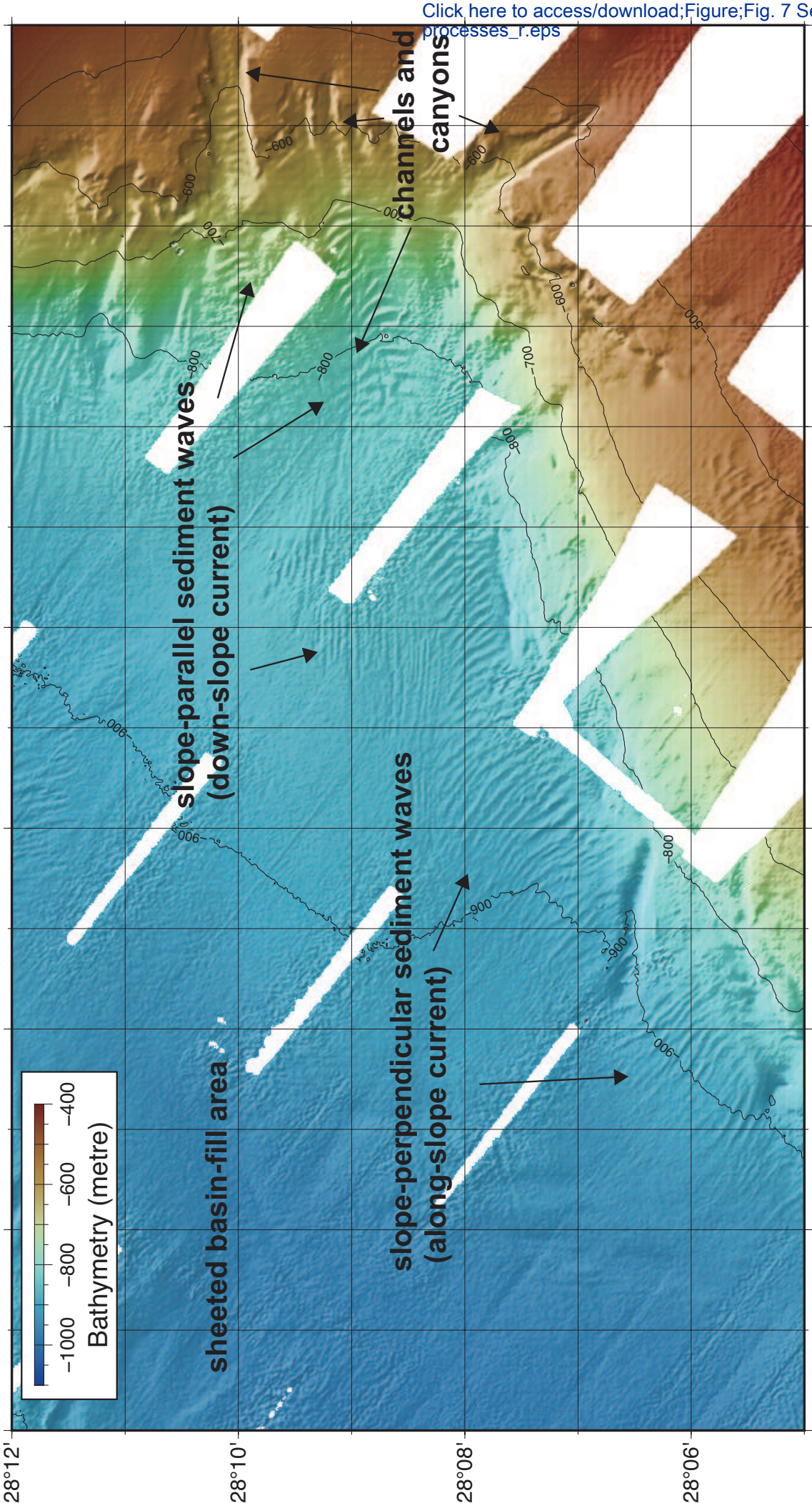

Figure 8

Figure 9

Figure 10

Click here to access/download;Figure;Fig. 10 Grain size vs. wavelength.eps

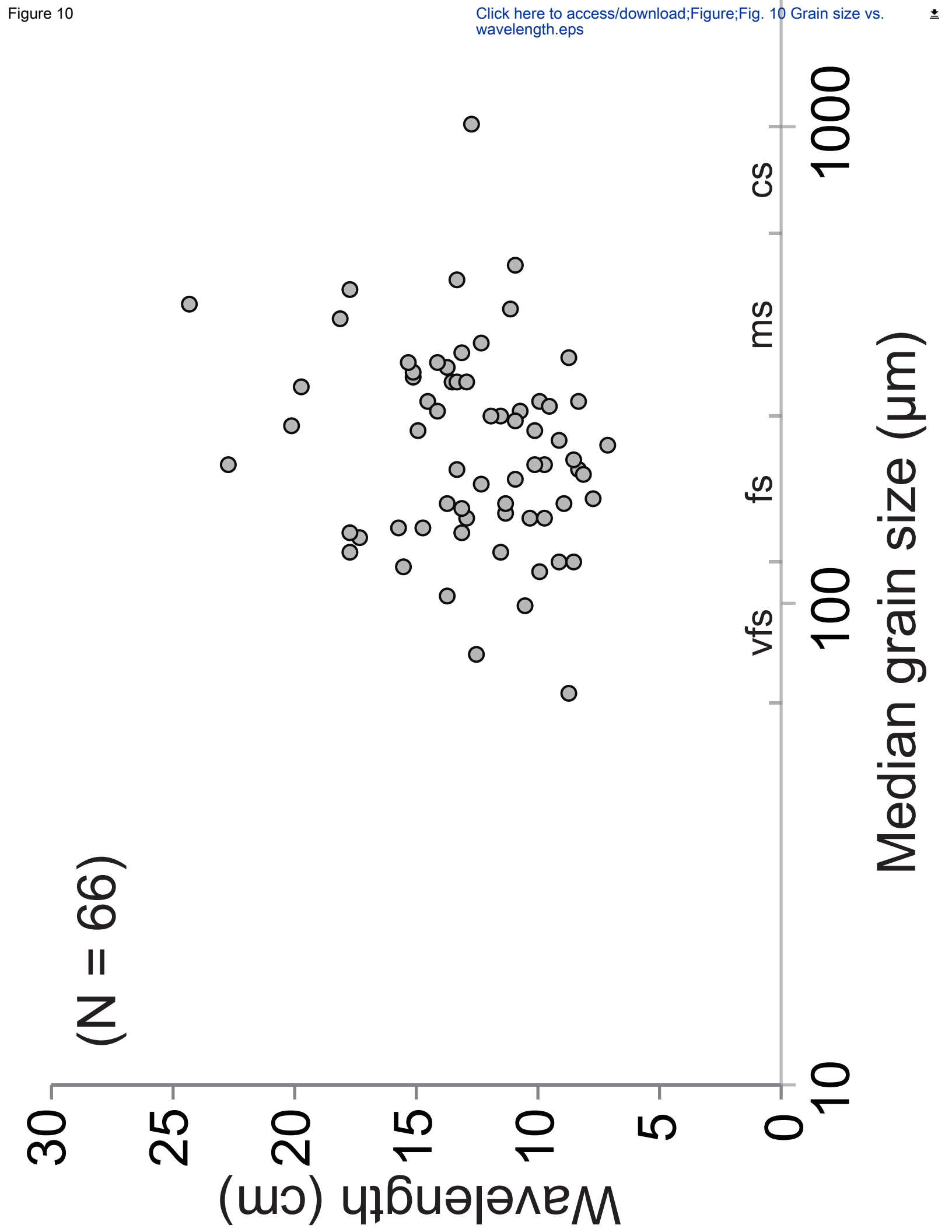

Table 1

Cruise	Station	Latitude (N)	Longitude (E)	Water depth (m)	Current direction/sense	Wavelength (cm)	Median grain size (mm)
GH08	18	25°48′46.80	127°17′49.20″	819	N30E–S30W	12.9	0.15
GH08	59	25°56′53.40	127°24′27.00″	331	N–S	12.2	0.18
GH08	60	26°00′30.60	127°19′12.00″	246	N20W–S20E	13.7	0.11
GH08	72	26°00′55.20	127°22′17.40″	260			0.13
GH08	84	26°03′41.40	127°21′51.00″	188	N70E–S70W	14.7	0.15
GH08	99	26°01′41.40	127°28′25.80″	234	N70E	14.9	0.30
GH08	100	26°04′04.80	127°24′55.20″	213	N90E	13.3	0.29
GH08	127	26°07′16.20	127°27′33.00″	138	N90E	9.8	0.27
GH09	152	26°06′51.60	127°35′27.00″	65	N65W	8.7	0.17
GH09	153	26°08′03.60	127°33′43.80″	68			0.41
GH09	154	26°09′16.20	127°31′57.00″	76	N80W–S80E	17.7	0.46
GH09	236	26°27′39.00	127°41′35.40″	466	N80E–S80W	17.3	0.14
GH09	242	26°44′58.80	127°20′10.80″	839	N75E–S75W	20.0	0.24
GH09	245	26°29′39.60	127°46′01.20″	409	S10E	24.1	0.43
GH09	256	26°31′18.00	127°47′22.80″	399	S70W		0.11
GH09	267	26°33′16.20	127°51′45.00″	294	S80W	13.2	0.30
GH09	302	26°50′32.40	127°41′13.20″	351			0.17
GH09	320	26°48′03.60	127°55′40.20″	312	S70E	15.0	0.31
GH09	326	26°48′27.60	127°58′49.20″	254	N10E	12.7	0.30
GH09	327	26°50′51.00	127°55′15.60″	252	N70E	12.9	0.15
GH09	330	26°55′39.60	127°48′16.20″	189			0.12
GH09	340	26°50′01.20	128°00′06.60″	275	N55E	10.5	0.25
GH09	358	26°50′58.80	128°06′10.80″	253	N	8.2	0.27
GH09	359	26°54′27.60	128°01′00.60″	347	S70W	8.1	0.20
GH09	384	26°58′58.80	128°09′01.20″	703	S55E	14.8	0.23
GH09	427	26°32′58.20	127°26′44.40″	627	S80W	14.3	0.27
GH09	430	26°39′27.60	127°21′00.00″	66			0.30
GH09	432	26°48′13.20	127°11′50.40″	841	N20E–S20W	15.6	0.15
GH09	439	26°48′12.00	127°22′47.40″	904	W	13.5	0.31
GH09	445	26°53′39.00	127°32′59.40″	720	N80E–S80W	9.3	0.27
GH09	446	26°53′42.00	127°43′59.40″	422	S10W	11.1	0.16
GH10	17	26°04′56.52	126°47′10.56″	1248	E–W	17.6	0.13
GH10	23	26°12′56.80	126°42′45.14″	954			0.13
GH10	29	26°14′33.21	126°44′04.39″	660			0.34
GH10	40	26°20′58.79	126°38′26.09″	593			1.00
GH10	46	26°12′56.07	126°53′45.76″	520	N70W–S70E	13.2	0.19
GH10	56	26°4′56.526	127°09′06.92″	428			0.20
GH10	58	26°24′9.312	126°41′07.54″	745	N60W–S60E	11.1	0.16
GH10	82	26°24′58.15	126°47′15.86″	587	N10W–S10E	12.3	0.08
GH10	144	26°16′90.59	127°18′22.04″	97			0.18
GH10	160	26°24′57.21	127°09′08.11″	524	S15E	18.0	0.40
GH10	161	26°27′21.16	127°05′38.72″	364	N55E–S55W	8.4	0.12
GH10	205	26°45′00.17	126°58′13.49″	764	N15W–S15E	17.6	0.14
GH10	230	26°44′58.34	127°09′11.65″	1132	N70W–S70E	19.5	0.29
GK12	463	27°02′24.84″	128°40′28.80″	862	S	13.5	0.17
GK12	487	27°17′35.94″	128°36′37.56″	362	S13E	8.5	0.33

GK12	489	27°18′52.80″	128°45′38.40″	652			
GK12	490	27°17′33.96″	128°47′31.74″	819	N45W	11.3	0.25
GK12	621	27°09′58.92″	127°16′27.72″	844	S45W–N45E	10.8	0.52
GK12	638	27°23′23.46″	128°08′26.46″	765	E	13.2	0.48
GK12	687	27°32′52.86″	127°59′41.82″	674	N60W–S60E		
GK12	699	27°34′28.20″	128°12′00.36″	823	S50W	9.5	0.20
GK12	709	27°41′39.72″	128°12′27.54″	685	E		
GK12	712	27°37′40.02″	128°03′39.30″	784	N	22.6	0.20
GK14	491	27°15′59.28″	128°52′21.78″	999	S55W–N55E		
GK14	567-2	27°02′27.72″	128°07′35.28″	622	S45E		
GK14	591	27°04′52.68″	127°53′04.62″	429	N80W–S80E		
GK14	640	27°19′17.82″	127°57′34.56″	570	N80W	10.8	0.24
GK14	703	27°41′08.52″	128°45′01.86″	805	W	11.8	0.25
GK14	725	27°43′57.00″	128°19′57.60″	620	N–S	14.0	0.33
GK14	744	27°54′23.16″	128°55′52.26″	65	E–W		
GK14	756	27°53′46.56″	128°16′53.94″	732	N25W–S25E		
GK15-2	524	27°35′46.74″	129°04′48.00″	445	S40E		0.12
GK15-2	531	27°41′52.80″	129°04′22.44″	342	E–W		0.16
GK15-2	533	27°43′09.72″	129°08′38.16″	473	N–S	10.2	0.15
GK15-2	540	27°46′21.72″	129°11′16.44″	611	N20E	7.0	0.22
GK15-2	541	27°45′32.40″	129°16′05.94″	971	N80E–S80W	7.5	0.17
GK15-2	551	27°52′47.40″	129°05′35.64″	440	N25W–S25E	11.0	0.42
GK15-2	553	27°53′33.30″	129°11′43.14″	617	N78E–S78W	8.3	0.20
GK15-2	555	27°55′08.64″	129°24′00.84″	610	N80E	9.6	0.16
GK15-2	560	27°57′34.62″	129°09′32.52″	226	N50E–S50W		0.38
GK15-2	562	27°59′09.48″	129°21′48.60″	293	N55E–S55W		0.17
GK15-2	563	27°59′56.22″	129°27′58.02″	542	N	11.3	0.13
GK15-2	762	27°58′41.22″	128°49′42.48″	793	N53W–E53W		0.40
GK15-2	808	27°44′21.60″	129°06′53.70″	354	E–W		0.17
GK15-2	824	28°01′30.96″	129°51′12.90″	1037	N–S	13.0	0.34
GK15-2	825	28°04′30.00″	129°25′00.90″	235			0.10
GK15-2	826	28°04′45.30″	129°31′56.52″	666	N80E–S80W	14.0	0.26
GK15-2	831	28°05′33.12″	129°38′04.32″	784			0.40
GK15-2	832	28°06′19.74″	129°44′13.44″	789			0.11
GK15-2	836	28°08′00.30″	129°49′06.72″	659	S60E	8.6	0.07
GK15-2	838	28°11′09.06″	129°37′13.68″	400	N40E–S40W	10.4	0.10
GK15-2	839	28°11′56.70″	129°43′22.20″	387	N80E–S80W	9.8	0.12
GK15-2	843	28°14′45.72″	129°31′59.88″	159	E–W	12.5	1.03
GK15-2	845	28°15′09.24″	129°46′02.52″	248	N55W–S55E	10.8	0.19
GK15-2	846	28°15′56.88″	129°52′11.40″	34	N40E–S40W		1.00
GK15-2	850	28°20′30.06″	129°38′20.10″	102	N20E–S20W	9.0	0.22
GK15-2	852	28°17′00.06″	130°01′35.16″	339	N30E–S30W	8.0	0.19
GK15-2	853	28°17′59.46″	130°07′26.04″	471	N10E–S10W	8.9	0.12
GK15-2	857	28°21′29.28″	129°56′47.76″	110	N55W–S55E	9.9	0.20
GK15-2	858	28°18′45.12″	130°02′45.60″	435	N–S		0.29
GK15-2	859	28°20′00.54″	130°04′31.74″	495			0.15
GK15-2	862	28°23′57.42″	129°58′47.70″	389	N20W–S20E		0.13
GK15-2	873	28°28′28.50″	130°14′00.48″	1839	N35E	15.4	0.12

GK15-2	884	28°28′49.86″	129°29′51.30″	206	N30W–E30E	10.0	0.23
GK15-2	894-3	28°33′30.60″	129°52′15.30″	260			0.40
GK15-2	899	28°38′26.64″	129°37′49.32″	472	N60E–S60W	12.2	0.35
GK15-2	912	28°43′16.56″	129°30′48.42″	704	N45E–S45W	15.1	0.32
GK15-2	913	28°44′03.60″	129°36′56.52″	699	N50E–S50W		0.17
GK15-2	922	28°48′00.00″	129°38′31.98″	736	N10E–S10W	13.0	0.16

Table 2: Sandy Contourite Systems

Name, location, references	Size (km^2) – approx. area	Water depth (m)	Sediments/bedforms	Depositional processes	Age
Shallow Water sandy contourites					
1. *Sao Tome* sand sheet, Campos slope, SW Atlantic (Viana et al., 1998)	2000	70–400	Siliciclastic (dominant) Bioclastic (secondary) Sand dunes and waves	Mixed	Holocene, but initiation in Neogene
2. *Sodwana* sand sheet, SW Atlantic (Flemming, 1980; Ramsay, 1994)	> 200	50–150	Siliciclastic Giant sand waves	Mixed	Holocene (initiation unknown)
3. *Adolphus* sand sheet, Grand Banks, NW Atlantic (Dalrymple et al., 1992)	> 100	60–200	Siliciclastic Sand and gravel waves, sand dunes and ribbons	Mixed	Late Pleistocene – Holocene
4. *Kozushima* sand sheet, Izu Ridge, NW Pacific (Kubo et al., 2004)	>150	200–400	Volcaniclastic Sand dunes, waves and ribbons; gravel and bare rock	Deep surface current, mixed	Holocene
Mid-depth sandy contourites					
5. *Cadiz* sand sheet Gulf of Cadiz, NE Atlantic (Stow et al., 2013a, b)	4000	400–800	Siliciclastic (minor bioclastic) Sand/gravel dunes, waves, ribbons, furrows	Bottom currents	Pliocene – Holocene
6. *Falkland* sand sheet Argentina, SW Atlantic (Nicholson and Stow, 2019)	30,000	1200–1800	Siliciclastic Sand waves, ribbons, giant crescentic scours	Bottom currents	Oligocene – Holocene
7. *Barra* sand sheet Hebrides slope, NE Atlantic (Stow et al., 2002c)	1000–1500	300–1200	Siliciclastic (minor bioclastic) Sand ripples, dunes	Bottom currents/Mixed	Late Pleistocene – Holocene
8. *Hebridean* sand sheet Hebrides slope, NE Atlantic (Howe et al., 1994)	1500	400–2000	Siliciclastic (minor bioclastic) Sand ripples, dunes	Bottom currents	Late Pleistocene – Holocene
9. *Florida Straits* sand sheet, NW Atlantic (Gardner et al., 1989)	150	600–800	Bioclastic Sand ripples, dunes, waves and ribbons	Bottom currents	Holocene (initiation unknown)

Deep-water sandy contourites					
10. *Carnegie Sand-Dune Valley*, E Pacific (Lonsdale and Malfait, 1974)	100	2650	Bioclastic Sand ripples, dunes	Bottom currents	Holocene (initiation unknown)
11*. Hatton flank* sand sheet, NE Atlantic (Stow and Holbrook, 1984)	3000–6000	2600–3200	Bioclastic Sand ripples, dunes	Bottom currents	Holocene (initiation unknown)
12. Ryukyu sand sheet, NW Pacific ***This study***	> 35,000	50– > 1500	Siliciclastic (dominant) Bioclastic (secondary) Sand ripples, dunes and sediment waves	Mixed	Late Pleistocene - Holocene